Available online at www.sciencedirect.com

ScienceDirect

Geochimica et Cosmochimica Acta 306 (2021) 1–19

Geochimica et Cosmochimica Acta

www.elsevier.com/locate/gca

Calcium isotope compositions of arc magmas: Implications for Ca and carbonate recycling in subduction zones

Jin-Ting Kang [a,b,*,1], Yu-Han Qi [a,c,1], Kan Li [c], Jiang-Hao Bai [d,e], Hui-Min Yu [a,b], Wang Zheng [f,g], Zhao-Feng Zhang [h], Fang Huang [a,b]

[a] *CAS Key Laboratory of Crust-Mantle Materials and Environments, School of Earth and Space Sciences, University of Science and Technology of China, Hefei 230026, China*

[b] *CAS Center for Excellence in Comparative Planetology, USTC, Hefei 230026, Anhui, China*

[c] *Earth and Atmospheric Sciences, University of Alberta, Edmonton, Alberta, Canada*

[d] *State Key Laboratory of Isotope Geochemistry, Guangzhou Institute of Geochemistry, the Chinese Academy of Sciences, Guangzhou 510640, China*

[e] *University of Chinese Academy of Sciences, Beijing, 100049, China*

[f] *Institute of Surface-Earth System Science, Tianjin University, Tianjin 300072, China*

[g] *School of Earth and Space Exploration, Arizona State University, Tempe, AZ 85287, USA*

[h] *International Center for Planetary Science, Chengdu University of Technology, Chengdu 610059, China*

Received 20 July 2020; accepted in revised form 7 May 2021; available online 19 May 2021

Abstract

Calcium (Ca) is a fluid-mobile element and plays a pivotal role in regulating carbon cycling through the precipitation of calcium carbonate. Calcium isotopes have been proposed as a promising tracer for deep carbon recycling because of the higher Ca content and distinctive Ca isotope composition in carbonate relative to the mantle. To test the effect of carbonate recycling on Ca isotope composition in arc magma and determine the fate of carbonate in subduction zones, we analyzed a suite of magmatic rocks from Central America, Southern Lesser Antilles, and Central-eastern Aleutian arcs. These three island arcs have variable thermal regimes from intermediate to cool and sediment types from carbonate-rich to carbonate-poor. Thirty-six arc magmas display $\delta^{44/40}$Ca values from 0.70‰ to 1.00‰ which are similar to the range of fresh mid-ocean ridge basalts (MORBs). Their average $\delta^{44/40}$Ca (0.82 ± 0.12‰, 2SD, n = 36) is lower than the estimates of Bulk Silicate Earth (~0.94‰, BSE) and can be ascribed to the effect of mantle partial melting. Despite strong evidence of C and Sr isotopes that various degrees of carbonate metasomatism occurred in the source of these rocks, they do not show Ca isotope variation. Based on the flux model, the buffering effect of the mantle wedge can homogenize the different carbonate Ca isotope signals at subduction zones where carbonate recycling efficiency is lower than 30% or the carbonates are mainly brought by carbonate-bearing altered oceanic crust. For subduction zones with carbonate recycling efficiency higher than 30%, the MORB-like $\delta^{44/40}$Ca in arc magmas may also reflect the storage of Ca in the mantle wedge and the retention of Ca in the descending slab beyond sub-arc depth. Combined with the fact that carbonate Ca isotope signals have been observed in OIBs and intra-plate igneous rocks, our new data indicates that most subducted Ca may finally enter the deep mantle via corner flow or within the descending slab.

© 2021 Elsevier Ltd. All rights reserved.

* Corresponding author at: CAS Key Laboratory of Crust-Mantle Materials and Environments, School of Earth and Space Sciences, University of Science and Technology of China, Hefei 230026, China.

E-mail address: kjt@ustc.edu.cn (J.-T. Kang).

[1] Co-first author.

https://doi.org/10.1016/j.gca.2021.05.014

0016-7037/© 2021 Elsevier Ltd. All rights reserved.

Keywords: Arc magmas; Carbonate recycling; Ca cycling; Ca isotope; Subduction Zone; Mantle wedge

1. INTRODUCTION

Megatons of Ca-rich carbonates in seafloor sediments and altered oceanic crust (AOC) are transferred into trenches every year (e.g., Alt and Teagle, 1999; Plank and Langmuir, 1998; Dasgupta and Hirschmann, 2010; Kelemen and Manning, 2015; Liu et al., 2019b; Plank and Manning, 2019). When the slab reaches the trench and descends, the prograde metamorphism splits the subducted carbonates into two fractions: one enters the Earth's convective mantle which further affects deep volatile recycling (e.g., Dasgupta et al., 2013; Burnham et al., 2015; Shirey et al., 2019), and the other returns to the surface primarily through arc volcanoes (e.g., Sano and Williams, 1996; Hilton et al., 2002). Therefore, the recycling of carbonate not only regulates atmospheric CO_2 concentration and global climate (e.g., Storey et al., 2007), but also influences the physicochemical properties of the mantle wedge (e.g., Foley, 2010; Li et al., 2017). This has motivated the development of various geochemical tracers such as Mg isotopes (e.g., Li et al., 2017) to identify and quantify the contribution of recycling carbonate to subduction zone.

Calcium is the most abundant cation in sedimentary carbonates ($CaCO_3$ or CaMg $(CO_3)_2$) and its isotopes have shown potential to be a tracer for carbonate recycling (e.g., Huang et al., 2011b; Amsellem et al., 2020; Sun et al., 2021). Carbonates in much of the Precambrian (3.0–0.54 Ga) have an average $\delta^{44/40}$Ca (see method part for the definition of $\delta^{44/40}$Ca) value similar to the composition of Bulk Silicate Earth (BSE) (Blättler and Higgins, 2017). However, $\delta^{44/40}$Ca of these sedimentary carbonates vary from BSE by ±0.7‰ and most of the biogenic carbonates formed after the Precambrian have lighter Ca isotope compositions (with an average of 0.6‰, Fantle and Tipper, 2014 and references therein) than the BSE estimates (~0.94‰, Kang et al., 2017; Chen et al., 2019). Therefore, the recycling of these sedimentary carbonates would alter the Ca isotope composition of the local mantle (e.g., Zhu et al., 2020b; Ionov et al., 2019). In addition, carbonate-bearing AOCs have heterogeneous Ca isotope compositions (0.49–1.31‰, Blättler and Higgins, 2017; Chen et al., 2020) due to the precipitation of carbonate veins, whereas fresh mid-ocean ridge basalts (MORBs) show a narrow range of $\delta^{44/40}$Ca (0.78–0.95‰, Zhu et al., 2018; Chen et al., 2020). Therefore, subducted carbonates are expected to have highly variable Ca isotope compositions and may modify the Ca isotope of arc magma.

Calcium isotope data, as yet, is only reported for back-arc basin basalts (BABBs) from south-western Pacific, Tonga, and Mariana, which have $\delta^{44/40}$Ca similar to the fresh MORB (Zhu et al., 2020a; Wang et al., 2021). Zhu et al. (2020a) attributed this signature to the low carbonate abundance in subducting sediments in the south-western Pacific. However, this explanation ignored the contribution of AOC, which can transfer large amounts of carbonates within sea-floor basalt as veins and vesicles (e.g., Alt and Teagle, 1999; Jarrard, 2003; Li et al., 2019). More importantly, Ca-rich carbonates are thought to be readily released at the fore-arc and sub-arc rather than the back-arc region (e.g., Frezzotti et al., 2011; Kelemen and Manning, 2015; Li et al., 2017). Therefore, in order to establish a closer link between the recycling of subducted carbonate and its Ca isotope effect on arc magma, more studies on representative rocks from volcanic-arc and fore-arc regions are required.

Here we present Ca isotope data for thirty-six representative arc magmas from Central-Eastern Aleutians, Central America, and Southern Lesser Antilles regions. Central America and Lesser Antilles subducting slabs are characterized by abundant carbonates in sedimentary layers, particularly for Central America, of which $CaCO_3$ abundance can reach up to 50 wt.% (Clift, 2017). In contrast, carbonates are mainly stored in AOC in Central-Eastern Aleutians with nearly no $CaCO_3$ in the sediments (Plank, 2014). Consequently, our sample set represents two end-member scenarios for subduction zones, which provides a valuable opportunity to assess the role of carbonate in modifying the Ca isotope budget of the mantle wedge. The purposes of this study are to (1) better understand the fate of carbonates in subduction zones; (2) investigate Ca cycling in the mantle wedge.

2. GEOLOGICAL BACKGROUND AND SAMPLE DESCRIPTION

2.1. The Lesser Antilles arc

The geological background of the Lesser Antilles arc has been thoroughly discussed in the literature (Devine and Sigurdsson, 1995; Turner et al., 1996; Hawkesworth et al., 1997; Macdonald et al., 2000 and references therein). Briefly, the Lesser Antilles arc is formed by westward subduction of the Atlantic oceanic lithosphere beneath the Caribbean plate. The convergence rate in the Southern Lesser Antilles (~1.3 cm/yr) is significantly slower than the north (3.7 cm/yr) because of the change in the obliquity of subduction (Jarrard, 1986; Speed et al., 1993). As a result, the subducting sedimentary columns in the Southern Lesser Antilles (~1750 m) are significantly thicker than the north (~235 m) (Plank, 2014).

Twelve samples were collected by dredging the crater environment of the Kick 'em-Jenny submarine volcano (12°300N, 61°380W) in the Southern Lesser Antilles (Devine, 1995; Sigurdsson and Shepherd, 1974), which is the only known active submarine volcano in the Lesser Antilles arc. In the past 100 years, Kick 'em-Jenny has erupted at least eight times (1939, 1943, 1953, 1965, twice in 1966, 1972, and 1974) (Shepherd and Robson, 1967). All the samples are fresh and lack associated organic material or calcareous detritus, suggesting that they are most likely derived from the 20th century eruptions (Sigurdsson and Shepherd, 1974). The olivine basalts from Kick 'em-

Jenny are highly porphyritic rocks with 25–50% phenocrysts of amphibole, plagioclase (An_{70}-An_{90}), clinopyroxene, and olivine (Fo_{70-85}). Plagioclase is a subordinate phenocryst phase and is invariably present as subdural crystals. Clinopyroxene phenocrysts are subordinate but always present as large euhedral individuals. Olivine phenocrysts are large and euhedral crystals and of very variable abundance in basalt. Iron-titanium oxides are an accessory micro-phenocryst phase. Photomicrographs can be found in Devine and Sigurdsson (1995). The major and trace element contents, Sr isotope compositions, and U-series data for these samples have been previously reported (Sigurdsson and Shepherd, 1974; Devine, 1995; Huang and Lundstrom, 2007; Huang et al., 2011). Their Sr isotope compositions illustrate moderate enrichment with $^{87}Sr/^{86}Sr$ from 0.70532 to 0.70632 (Huang et al., 2011a), which are significantly higher than the Northern Lesser Antilles lavas and suggest a greater contribution of the sedimentary components in Kick'em-Jenny lava (Turner et al., 1996; Macdonald et al., 2000). The low Ba/Th ratio (Fig. 2) and elevated Ta/Zr in Kick'em-Jenny lava indicate that the sedimentary components may be in the form of partial melts (Turner et al., 1996).

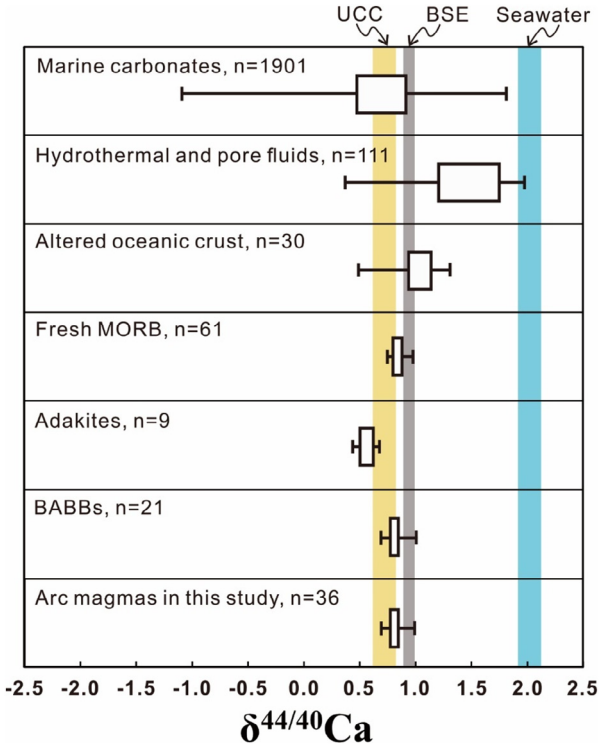

Fig. 1. The $\delta^{44/40}Ca$ of arc magmas examined in this study. The $\delta^{44/40}Ca$ range of marine carbonate sediments (Blättler and Higgins, 2017; Fantle and Tipper, 2014 and reference therein), hydrothermal and pore fluids (from the compilations in Fantle and Tipper, 2014), AOCs (Blättler and Higgins, 2017; Chen et al., 2020), fresh MORBs (Chen et al., 2020; Zhu et al., 2018), adakites (Wang et al., 2019) and BABBs (Zhu et al., 2020a) are shown for comparison. The gray bar represents the estimated $\delta^{44/40}Ca$ of BSE of 0.94 ± 0.05‰ (Kang et al., 2017). The yellow bar represents the estimated $\delta^{44/40}Ca$ of the upper continental crust of 0.72 ± 0.10‰ (Wang et al., 2019). The blue bar represents the $\delta^{44/40}Ca$ of seawater of 1.90 ± 0.18‰ (from the compilations in Fantle and Tipper, 2014). (For interpretation of the references to colour in this figure legend, the reader is referred to the web version of this article.)

2.2. Central Eastern Aleutians

The Aleutian arc is formed by the subduction of the Pacific plate beneath the American plate (Tibaldi and Bonali, 2017 and references therein; Yogodzinski et al., 1995). It is comprised of three parts: the Western, Central, and Eastern segments (Yogodzinski et al., 1995; Cai et al., 2015). The Western Aleutians (west of 180°W) extend from the Komandorsky Islands to the eastern end of the Rat Islands, and the Central Eastern Aleutians (east of 180° W) extend from the Delarof Islands to the western end of the Alaskan Peninsula (Cai et al., 2015).

Both intrusive and extrusive rocks can be located in Central-Eastern Aleutians. The tholeiitic lavas have younger ages, dating to the Holocene, and are exposed on the older calc-alkaline plutons with Eocene to Miocene (39–9 Ma) age (Cai et al., 2015). The plutonic rocks are thought to represent magma composition rather than crystal cumulates (Cai et al., 2015). This is attributed to the fact that they have negligible Eu anomalies, similar or higher $Na_2O + K_2O$, and similar or lower CaO and Al_2O_3 compared with lavas at a given Mg#. The major and trace element compositions of plutonic rocks strongly resemble the calc-alkaline Holocene lavas with more depleted Sr-Nd-Pb-Hf isotope ratios in the Western Aleutians (Cai et al., 2015 and references therein). Specifically, the plutonic rocks from the Central-Eastern Aleutians are characterized by MORB-like $^{87}Sr/^{86}Sr$ ratio and high ε_{Nd} (>7.5) and ε_{Hf} (>13) coupled with higher Th/Nd and Hf/Lu compared with the depleted MORB mantle (DMM). These geochemical features have been ascribed to the addition of low degree partial melts of subducted oceanic crust in an eclogite phase and minor amounts of subducted sediments (Cai et al., 2014, 2015; Yogodzinski et al., 2015). The sedimentary columns in the Central-Eastern Aleutians are primarily composed of ashy-siliceous clay and turbidites with nearly no carbonate (Plank, 2014).

Eight calc-alkaline plutonic rocks (diorite and granodiorite) are from the Atka and Umnak islands and one andesite is from the Umnak Island. Most of the intrusive rocks are fine-grained (<1 mm) and consist primarily of lath shaped plagioclase, anhedral quartz, orthopyroxene, amphibole, biotite, and potassium feldspar. Lesser amounts of anhedral titanomagnetite, subhedral to euhedral clinopyroxene, and separate actinolite grains also occur (e.g., Kay et al., 1983). Their petrology, major and trace element contents, and Zn-Sr-Nd-Pb-Hf isotope compositions have been previously reported (Cai et al., 2015; Huang et al., 2018).

2.3. The Central American volcanic arc

The Central American volcanic arc system extends from western Guatemala to Central Panama, and the present volcanic front comprises well-defined stratovolcanoes and

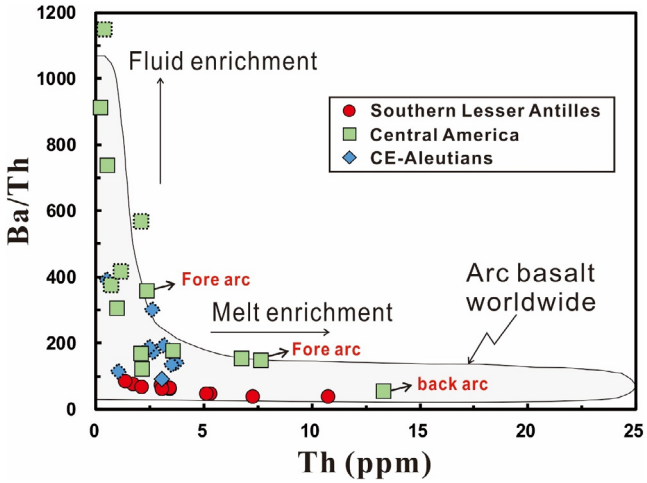

Fig. 2. Arc magmas from Southern Lesser Antilles, Central-Eastern Aleutians, and Central America in this study compared to other arc systems in Ba/Th vs. Th. Data of arc magmas worldwide are from the compilations in Drummond and Defant (1990) and Hawkesworth et al. (1997). Symbols with dashed borders represent intrusive rocks and solid borders for extrusive rocks.

related eruptive centers (e.g., Carr, 1984; de Boer et al., 1988; Herrstrom et al., 1995). The modern arc is created by the convergence between the Caribbean Plate and the subducting Cocos Plate and a remnant of the Nazca Plate. The sedimentary columns in the Central America arc are predominantly composed of carbonate and have the highest bulk CaO content (~34.59 wt.%) among the global arcs (Plank, 2014).

Seven out of sixteen samples, including five volcanics (basaltic andesite, andesite, and dacite) and two plutonic rocks (gabbro and granodiorite), are derived from western and southern Panama (four are from the Chagres-Bayano arc, two are from the Cordilleran arc, and one is from the Soná-Azuero arc). Most samples are fresh but some exhibit minor degrees of alteration (Wegner et al., 2011). Their petrology, major and trace element compositions, O-Sr-Nd-Pb isotope compositions, and ^{40}Ar-^{39}Ar ages (0.39–70 Ma) were reported by Wegner et al. (2011).

Six volcanics (basalt to andesite) and two plutonic rocks (gabbro and tonalite) are from Costa Rica, including five samples from the central magmatic arc, two from the fore-arc region (PAS-74 and PAS-75), and one from the back-arc region (BRI-21) (Abratis and Wörner, 2001). Most samples are fresh (Abratis and Wörner, 2001). The principal phenocrysts in volcanics are pyroxenes and plagioclases, which usually occurred as euhedral crystals. Olivine is a subordinate phenocryst phase and minor amounts of amphibole also can be found (Abratis and Wörner, 2001). The back-arc rock displays a low Ba/Th ratio (Fig. 2), indicating an insignificant contribution of slab fluids to its mantle source (Abratis and Wörner, 2001). Samples from the central magmatic arc and fore-arc regions are characterized by depletion in Nb and Ta and enrichment of fluid-mobile elements such as Ba, K, Pb, and Sr, suggesting the addition of variable amounts of slab fluids (Fig. 2). Their moderately enriched Sr-Nd-Pb isotope compositions indicate the incorporation of sediment components in their mantle source(Abratis and Wörner, 2001Wegner et al., 2011).

3. ANALYTICAL METHODS

Rocks were first crushed into separates with a diameter smaller than 5 mm. Volcanics were handpicked under the binocular microscope to remove separates containing phenocrysts (if any). Then, they were ultrasonically washed for 30 minutes using MQ-water in preparation for acid digestion. Calcium isotope composition is reported relative to NIST SRM915a as: $\delta^{44/40}Ca = [(^{44}Ca/^{40}Ca)_{sample}/(^{44}Ca/^{40}Ca)_{NIST\ SRM915a} - 1]$ (‰). Notably, ^{40}Ca is one of two daughter products from the branched decay of ^{40}K (half-life 1.397×10^9 years, Steiger and Jäger 1977). Therefore, radiogenic ^{40}Ca contribution could be significant in old rocks with high K/Ca. Given the high K/Ca ratios and old ages for samples from Central-Eastern Aleutians (average K/Ca = 0.79 and 9–39 Ma) and Central America (average K/Ca = 0.20 and 0.39–70 Ma), the directly measured $\delta^{44/40}$Ca may reflect the net effect of ^{40}K decaying and stable isotope fractionation. To avoid interferences from ^{40}K decaying, Central-Eastern Aleutians and Central America samples were measured for $\delta^{44/42}$Ca ($\delta^{44/42}Ca = [(^{44}Ca/^{42}Ca)_{sample}/(^{44}Ca/^{42}Ca)_{NIST\ SRM\ 915a} - 1]$ (‰)) on multiple-collector inductively coupled plasma mass spectrometry (MC-ICP-MS). On the other hand, the $\delta^{44/40}$Ca of Southern Lesser Antilles were directly measured by thermal ionization mass spectrometry (TIMS) because of their low K/Ca ratios (with an average value of 0.12) and very young age (<100 years). Additionally, the $\delta^{44/40}$Ca of Central-Eastern Aleutians samples were also directly measured by TIMS to evaluate the possible ^{40}K decaying effect in arc magmas. The details of the two methods are briefly described as follows.

3.1. Ca isotope analyses on MC-ICP-MS

Chemical procedure and mass spectrometric analysis for samples from Central-Eastern Aleutians and Central America were completed at Arizona State University (ASU) using the Neptune multi-collector (MC) ICP-MS (Thermo

Scientific). Specifically, 10–60 mg of rock powder was digested using HF + HNO_3 (5:1) in a 7 ml PFA beaker on a hot plate at 110 °C for 2–3 days. After the digestion, the samples were dried down at 80 °C and refluxed with 6 M HCl several times until completely dissolved to remove precipitated CaF_2, then evaporated to dryness. Subsequently, the dried material was dissolved in 2 M HNO_3 for column chemistry. Separation of Ca from the sample matrix was automatically performed using the prepFAST MC (ESI) and the supplied 1 ml Sr–Ca column (part number CF-MC-SrCa-1000) following the method of Romaniello et al. (2015). The Ca yields in the column chemistry were from 90% to 93%. No detectable Ca isotope fractionation was observed if the Ca yields are as low as 75% (Romaniello et al., 2015). Calcium isotope compositions were measured using a MC-ICP-MS equipped with a Jet sample cone, an H-skimmer cone, and an Apex-Q desolvating nebulizer (ESI). Measurements were done using the ^{43}Ca-^{46}Ca double spike method with sample-standard bracketing (DS-SSB-MC-ICP-MS, see details in Ionov et al., 2019). The double-spike solution was added as 2% of the total Ca concentration in samples ≥24 h before the isotope analysis to allow full spike-sample equilibration. Faraday cups were positioned to measure $^{42}Ca^+$, $^{43}Ca^+$, $^{44}Ca^+$, $^{45}Sc^+$, $^{46}Ca^+$, $^{47}Ti^+$, and $^{48}Ca^+$. Details of the cup configuration and interference corrections are specified by Romaniello et al. (2015). Moreover, double-spiked Ca samples were applied in sequential order with every two samples bracketed by the equivalently spiked ICP1 in-house standard. Additionally, mass bias and corrected isotope ratios were calculated using the Newton-Rhapson procedure (Albarède and Beard, 2004). The Ca isotope ratio was calculated in delta notation: $\delta^{44/42}Ca = [(^{44}Ca/^{42}Ca)_{sample}/(^{44}Ca/^{42}Ca)_{ICP1} - 1]$ (‰), and was normalized against an international reference material NIST SRM915a. This in turn was purified and double-spiked using the same procedure as the samples. The final data was reported as $\delta^{44/40}Ca_{SRM915a}$ by multiplying $\delta^{44/42}Ca_{SRM915a}$ with a scaling factor of 2.0483 based on the kinetic mass-dependent fractionation law (Young et al., 2002). Notably, all samples were measured at least 3 times. Throughout the course of this study, long-term external precision (2SD of $\delta^{44/42}Ca$) was 0.08‰ (n = 24), and the precision of $\delta^{44/40}Ca$ can be propagated by 0.08‰ × 2.0483 ≈ 0.16‰. The $\delta^{44/40}Ca$ values (relative to SRM915a) for BCR-2 and BIR-1 in the same session are 0.90 ± 0.12‰ (2SD, n = 3) and 0.76 ± 0.12‰ (2SD, n = 3) (Table S1). These results are consistent with that reported in previous studies (Amsellem et al., 2017; Chen et al., 2019; Feng et al., 2017; Liu et al., 2017b; Valdes et al., 2014; Wombacher et al., 2008) and the values obtained by TIMS in this study (Table S1). Additionally, full duplicates of sample PAS-74 obtained by digestion of two batches of powder were reproduced within the analytical error (Table 1).

3.2. Ca isotopes analyses on TIMS

The chemical procedure and analysis for samples from Southern Lesser Antilles were implemented on the TIMS (Thermo Triton) in the State Key Laboratory of Isotope Geochemistry, Guangzhou Institute of Geochemistry (GIG), and the Chinese Academy of Sciences (CAS). This was completed following the procedure described by Liu et al. (2019a) and references therein. Briefly, approximately 10 mg of sample powder was digested by a mixture of concentrated HF and HNO_3 (3:1) in a 7 ml Teflon beaker on a hot plate. After the digestion, the sample was dried down at 80 °C and refluxed with 6 M HCl several times until completely dissolved to remove precipitated CaF_2, then evaporated to dryness. This dried residue was finally dissolved in 1.6 N HCl. Prior to the chemical purification, an aliquot containing ~50 μg Ca was mixed with a ^{42}Ca-^{43}Ca double spike. The mixture was dried down and dissolved in 0.05 ml of 1.6 M HCl for column chemistry. Notably, calcium was purified using a Teflon micro-column filled with 1 ml of AG MP-50 (100–200 mesh) resin with 1.6 M HCl. The Ca yields was generally >99%. To access its reproducibility and quality, at least one reference material and blank were processed as unknown samples for each batch of column chemistry. The total procedure blank was less than 100 ng, which was negligible compared to the 50 μg of Ca loaded onto the column. Calcium isotope compositions were measured on a Triton TIMS. The ^{41}K was monitored to correct for ^{40}K interference on ^{40}Ca using $^{40}K/^{41}K = 1.7384 \times 10^{-3}$ (Heuser et al., 2002). Additionally, instrumental fractionation was corrected by the ^{42}Ca-^{43}Ca double spike technique by applying an iterative algorithm with an exponential law. Two standard deviations of $\delta^{44/40}Ca$ in SRM915a measured throughout the course of this study is ±0.13‰ (n = 32), which represents long-term external precision. During the run, the $\delta^{44/40}Ca$ for BCR-2 and BIR-1 are 0.81 ± 0.09‰ (2SD, n = 3) and 0.85 ± 0.09‰ (2SD, n = 3), respectively, which agree with the values measured by DS-SSB-MC-ICP-MS of this study and data reported in the literature (Table S1). Specifically, duplicates of KEJ-89-9, KEJ-101, RB47, and RB65 obtained by digestion of the two batches of powder were reproduced within the analytical error (Table 1).

4. RESULTS

The Ca isotope data are listed in Table 1. The $\delta^{44/40}Ca$ values of Central-Eastern Aleutians samples obtained by DS-TIMS and DS-SSB-MC-ICP-MS are plotted against each other in Fig S1. All the data points fall close on the 1:1 line, indicating that ^{40}K decaying has an insignificant effect on $\delta^{44/40}Ca$ of Central-Eastern Aleutians samples. It also suggests that the data obtained by DS-TIMS and DS-SSB-MC-ICP-MS are comparable and both of high quality. In order to maintain consistency with Central American rocks which also have a high K/Ca ratio and old age, we used the values measured by DS-SSB-MC-ICP-MS for Central-Eastern Aleutians samples in the following discussions.

The studied arc magmas from Southern Lesser Antilles, Central-Eastern Aleutians, and Central America arcs have $\delta^{44/40}Ca$ from 0.70 ± 0.14‰ to 1.00 ± 0.02‰, with an average of 0.82 ± 0.12‰ (2SD, n = 36). Notably, this value is lower than the composition of the fertile mantle (0.94–1.05‰, Huang et al., 2010; Kang et al., 2017; Chen et al.,

Table 1
Ca isotope compositions of arc magmas.

Location	Sample#	Rock type	By DS-TIMS				By SSB-DS-MC-ICP-MS				n[b]
			$\delta^{44/42}$Ca	2SD[a]	$\delta^{44/40}$Ca	2SD[a]	$\delta^{44/42}$Ca	2SD[a]	$\delta^{44/40}$Ca	2SD[a]	
Southern Lesser Antilles											3
Kick'em Jenny	RB51b	Basalt	0.39	0.06	0.81	0.12					3
Kick'em Jenny	KEJ-89-9	Basalt	0.40	0.05	0.82	0.10					1
	Repeat[c]		0.45	0.92							3
Kick'em Jenny	KEJ-010	Basaltic Andesite	0.34	0.07	0.70	0.14					3
Kick'em Jenny	KEJ-103	Basaltic Andesite	0.41	0.06	0.84	0.13					3
Kick'em Jenny	RB64	Basalt	0.42	0.03	0.87	0.07					3
Kick'em Jenny	RB82	Basalt	0.40	0.05	0.83	0.11					3
Kick'em Jenny	RB07	Basaltic Andesite	0.38	0.05	0.78	0.11					3
Kick'em Jenny	KEJ-101	Basalt	0.40	0.03	0.81	0.07					1
	Repeat[c]		0.41	0.83							3
Kick'em Jenny	RB79	Basalt	0.40	0.07	0.82	0.14					3
Kick'em Jenny	RB47	Andesite	0.40	0.07	0.82	0.14					1
	Repeat[c]		0.41	0.83							3
Kick'em Jenny	RB65	Basalt	0.38	0.03	0.78	0.07					1
	Repeat[c]		0.39	0.80							3
Kick'em Jenny	KEJ-100	Basalt	0.42	0.05	0.87	0.10					
Central-Eastern Aleutians											
Atka	877–12-8	Diorite	0.39	0.04	0.80	0.08	0.41	0.02	0.83	0.04	3
Atka	877–14-5II	Diorite	0.41	0.02	0.84	0.05	0.42	0.04	0.86	0.09	3
Atka	877–15-1′	Diorite	0.44	0.03	0.91	0.06	0.43	0.06	0.88	0.13	3
Atka	877–15-4	Diorite	0.41	0.06	0.84	0.12	0.41	0.02	0.85	0.05	3
Atka	877–16-6	Granodiorite	0.42	0.05	0.86	0.10	0.46	0.05	0.95	0.11	3
Umnak	47ABy3	Diorite	0.39	0.04	0.79	0.09	0.38	0.03	0.78	0.07	3
Umnak	47ABy31	Andesite	0.46	0.06	0.94	0.12	0.49	0.01	1.00	0.02	3
Umnak	47ABy34	Diorite	0.44	0.04	0.91	0.08	0.43	0.06	0.88	0.12	3
Umnak	47ABy41	Diorite	0.41	0.06	0.84	0.12	0.39	0.01	0.80	0.03	3
Central America							0.42	0.03	0.85	0.07	3
Costa Rica	ALT-14	Basalt					0.40	0.05	0.82	0.10	3
Costa Rica	CHI-113	Basaltic andesite					0.36	0.05	0.74	0.11	3
Costa Rica	NUE-92	Gabbro					0.35	0.03	0.71	0.07	3
Costa Rica	CHI-116	Tonalite					0.36	0.01	0.73	0.02	3
Costa Rica	BRI-21	Basalt					0.36	0.03	0.74	0.06	3
Costa Rica	PAS-74	Baslatic trachyand					0.35	0.02	0.72	0.04	3
	Repeat[c]										
Costa Rica	PAS-75	Basalt					0.37	0.09	0.76	0.19	5
Costa Rica	TUR-64	Trachyandesite					0.37	0.06	0.76	0.11	3
Panama	PAN-03-007	Gabbro					0.39	0.01	0.81	0.02	3
Panama	PAN-03-022	Granodiorite					0.44	0.07	0.90	0.15	3
Panama	PAN-03-023	Andesite					0.38	0.04	0.78	0.08	3
Panama	PAN-04-004	Andesite					0.42	0.03	0.86	0.05	3

Panama	PAN-05-008	Dacite	0.41	0.08	0.84	0.16	4	
Panama	PAN-05-056	Basaltic andesite	0.41	0.06	0.85	0.13	3	
Panama	PAN-06-131	Dacite	0.39	0.08	0.80	0.16	3	

[a] 2SD = two standard deviations.
[b] n represents the times of repeat isotope measurements for the same purified solution.
[c] Repeat = repeated the whole procedure, including sample dissolution, column chemistry and mass spectrometry.

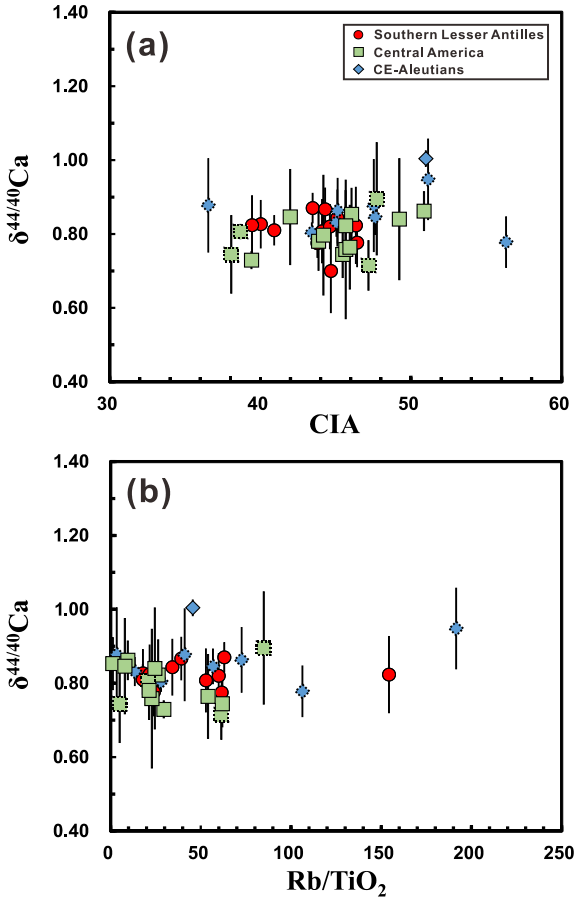

Fig. 3. The $\delta^{44/40}$Ca of arc magmas from Southern Lesser Antilles, Central-Eastern Aleutians, and Central America vs. (a) CIA and (b) Rb/TiO_2. Symbols with dashed borders represent intrusive rocks and solid borders for extrusive rocks.

2019; Amsellem et al., 2019) and comparable to the average value of BABBs (0.80 ± 0.08‰, 2SD, n = 21) from the southwestern Pacific (Zhu et al., 2020a) and of fresh MORBs (0.83 ± 0.11‰, 2SD, n = 21; Chen et al., 2020; Zhu et al., 2018). Surprisingly, there is no systematic across-arc Ca isotope difference with an average $\delta^{44/40}$Ca of 0.81 ± 0.09‰ for Southern Lesser Antilles, 0.87 ± 0.14‰ for Central-Eastern Aleutians, and 0.80 ± 0.11‰ for Central America, respectively. In addition, no Ca isotope variation is observed in rocks from the fore-arc (0.74–0.76‰), volcanic arc (0.71–0.85‰), and back-arc regions (0.73‰) in Central America.

5. DISCUSSION

5.1. Calcium isotope composition of arc magmas

Arc magmas from Central America, Southern Lesser Antilles, and Central-Eastern Aleutians reveal a homogenous Ca isotope composition (0.82 ± 0.12‰, 2SD, n = 36) which is about 0.1‰ lighter than that of the fertile mantle (0.94–1.05‰, Huang et al., 2010; Kang et al., 2017; Chen et al., 2019; Amsellem et al., 2019). Several factors

may account for this including post-magmatic alteration (e.g., Jacobson et al., 2015; Tipper et al., 2016), crustal contamination (Banerjee and Chakrabarti, 2019; Wang et al., 2019), fractional crystallization (e.g., Valdes et al., 2019), mantle partial melting (e.g., Kang et al., 2017), and incorporation of subduction carbonates (e.g., Huang et al., 2011b; Amsellem et al., 2020).

Most rocks in this study are fresh as evidenced by the absence of associated organic material or calcareous detritus (Sigurdsson and Shepherd, 1974) and the existence of non-devitrified glass (Abratis and Wörner, 2001). Their Chemical Index of Alteration (i.e., CIA, $[Al_2O_3/(Al_2O_3 + CaO + Na_2O + K_2O)] \times 100$) mostly falls in the range of fresh igneous rock (<50, Nesbitt and Young, 1982). Although section examination has revealed minor degrees of secondary alteration in a few samples (Wegner et al., 2011), the absence of correlation between $\delta^{44/40}$Ca with CIA and with Rb/TiO_2 ratio ruled out the effect of post-magmatic alteration (Fig. 3). Central America, Southern Lesser Antilles, and Central-Eastern Aleutians arc magmas experienced various degrees of crustal contamination because their Ti/Zr and Nb/La ratios are lower than those of N-MORB (Fig S2). However, the absence of correlation between $\delta^{44/40}$Ca and Ti/Zr or Nb/La (Fig. 4a and b) precludes the isotope effect induced by crustal contamination.

The Ca isotope compositions of these samples are not controlled by fractional crystallization either. These arc magmas display a wide range in major element concentra-

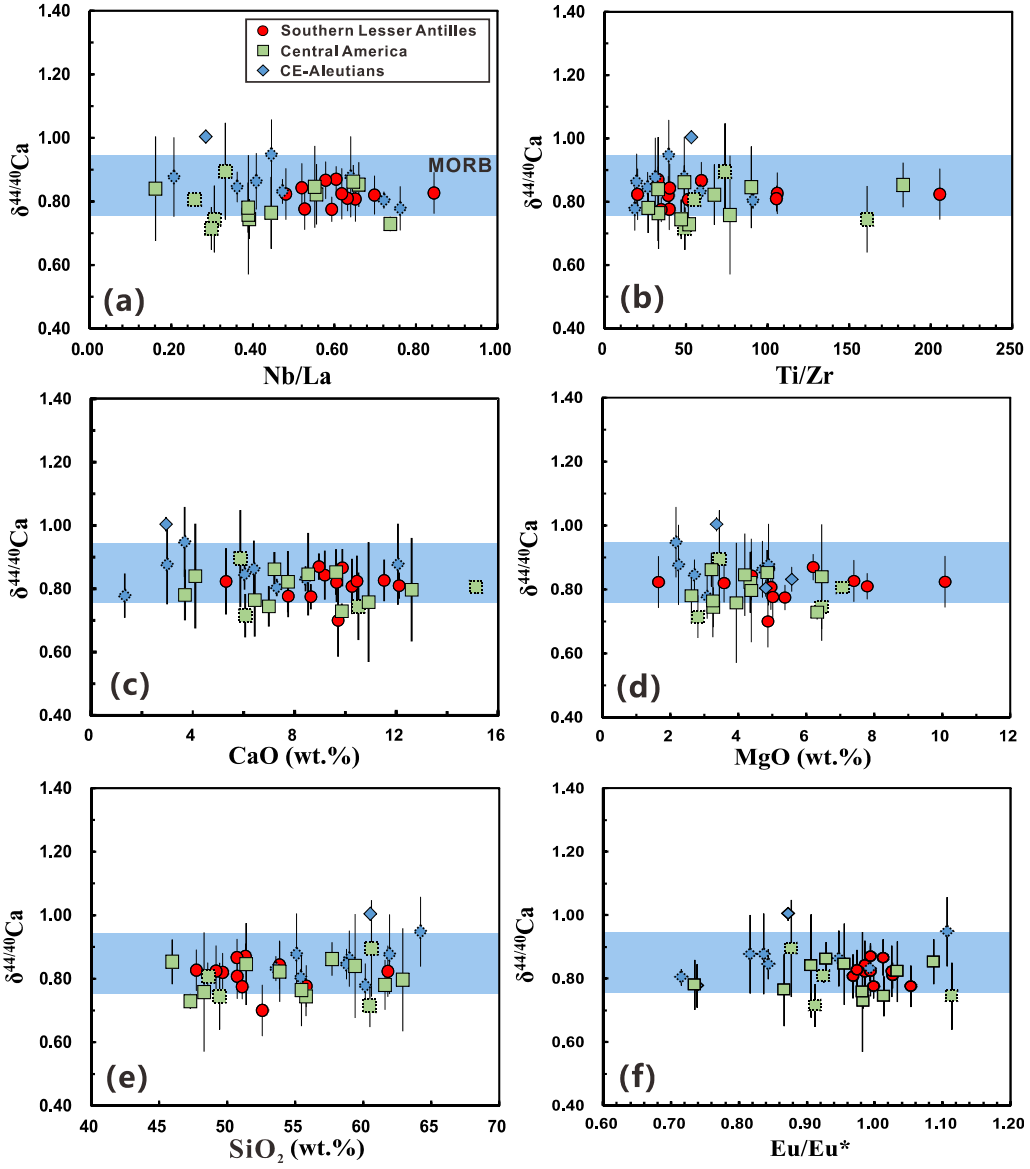

Fig. 4. $\delta^{44/40}$Ca of arc magmas versus (a) Nb/La, (b) Ti/Zr, (c) CaO wt.%, (d) MgO wt.%, (e) SiO_2 wt.%, and (f) Eu/Eu*. The $\delta^{44/40}$Ca range of fresh MORBs (Chen et al., 2020; Zhu et al., 2018) is shown as the blue bar. Symbols with dashed borders represent intrusive rocks and solid borders for extrusive rocks. (For interpretation of the references to colour in this figure legend, the reader is referred to the web version of this article.)

tions, with MgO from 2.62 wt.% to 10.08 wt.%, CaO/Al_2O_3 from 0.07 to 0.7 and FeO from 2.44 wt.% to 11.8 wt.% (Fig S3), suggesting the fractionation of the assemblage of olivine + clinopyroxene + orthopyroxene + plagioclase + magnetite + amphibole occurred (Heath et al., 1998; Macdonald et al., 2000; Sigurdsson and Shepherd, 1974; Abratis and Wörner, 2001). Given the low CaO content in magnetite (~0.14 wt.%) and its low mass fraction in the crystallized assemblage (<6%, Heath et al., 1998), magnetite fractional crystallization should introduce minor Ca isotope fractionation. Similarly, olivine and orthopyroxene may have limited Ca isotope effect due to their low CaO content (<0.1 wt.% for olivine and <1 wt.% for orthopyroxene), although olivine and orthopyroxene may have heavier Ca isotope composition than silicate melt (e.g., Chen et al., 2019; Huang et al., 2019; Kang et al., 2016). Clinopyroxene, plagioclase, and amphibole, which have CaO content of ~20 wt.%, ~10 wt.%, and ~11.5 wt.% respectively, are the main carriers of Ca in crystallized assemblages. A recent study by Valdes et al. (2019) found large Ca isotope variations (−1.6 to 1.8‰) in the layered igneous complex from the West African craton, suggesting a possible effect caused by plagioclase and amphibole fractional crystallization. However, regarding samples in this study, there is no correlation between $\delta^{44/40}Ca$ and magma evolution indicators like CaO, MgO, SiO_2, and Eu/Eu* (Fig. 4). These signatures indicate that Ca isotopes are resilient to the fractional crystallization of clinopyroxene, plagioclase, and amphibole in basaltic and andesitic magmas. Similarly, the absence of Ca isotope fractionation during fractional crystallization has been observed in OIBs from Hawaii (Huang et al., 2011b; Zhang et al., 2018), global MORBs (Zhu et al., 2018; Chen et al., 2020), BABBs from southwestern Pacific (Zhu et al., 2020a), and granitoids from Dabie orogen (Wang et al., 2019).

The $\delta^{44/40}Ca$ offset between arc magmas and fertile mantle should alternatively reflect the fractionation induced by mantle partial melting. Previous determination of fresh MORBs found lower $\delta^{44/40}Ca$ (~0.83‰) than DMM, which is ascribed to the effect of mantle partial melting (Kang

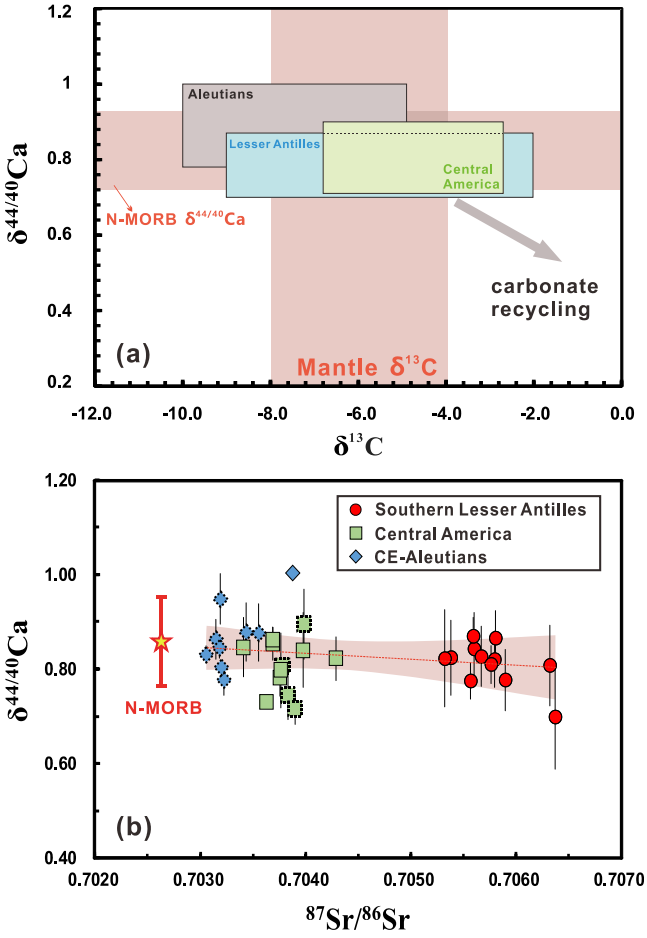

Fig. 5. $\delta^{44/40}Ca$ versus and $\delta^{13}C$ (a) and $^{87}Sr/^{86}Sr$ (b) for arc magmas from Southern Lesser Antilles, Central-Eastern Aleutians, and Central America. The carbon isotope compositions of the three arcs are from the compilations in Mason et al., 2017. The $\delta^{13}C$ of mantle is from Howell et al. (2020) (−8 to −4‰). Regression line (red dashed line) with the 95% C. I. envelope (pink area) is shown. The $\delta^{44/40}Ca$ of N-MORB is from Zhu et al. (2018) and Chen et al. (2020) and the $^{87}Sr/^{86}Sr$ of N-MORB is 0.702630 from Salters and Stracke (2004). Symbols with dashed borders represent intrusive rocks and solid borders for extrusive rocks. (For interpretation of the references to colour in this figure legend, the reader is referred to the web version of this article.)

et al., 2017; Zhu et al., 2018; Chen et al., 2020). This stems from the incongruent melting of mantle minerals. The $\delta^{44/40}$Ca in mantle minerals generally follow the order of olivine ≥ orthopyroxene > clinopyroxene (e.g., Kang et al., 2016, 2020). Clinopyroxene accounts for more than 90% of the Ca budget in fertile peridotites and will be consumed by partial melting at a rate faster than olivine and orthopyroxene (e.g., Pickering-Witter and Johnston, 2000). With the increasing degree of melt extraction, the abundances of orthopyroxene and olivine in residue increase and lead to the enrichment of heavy Ca isotope in melt-depleted harzburgites (e.g., Kang et al., 2017). Therefore, partial melts derived from a fertile mantle source will have lighter Ca isotope compositions (e.g., Kang et al., 2017, 2019; Chen et al., 2019). Numerical modelings in previous studies suggest that the $\delta^{44/40}$Ca of partial melts may be 0–0.1‰ lighter than the fertile mantle (Chen et al., 2019; Kang et al., 2017; Zhang et al., 2018; Zhu et al., 2020a). Consistent with these modeling results, the average $\delta^{44/40}$Ca of arc magmas (0.82 ± 0.12‰) is about 0.12‰ lower than the fertile mantle (0.94–1.05‰) and is comparable with that of fresh MORBs (0.83 ± 0.11‰, Chen et al., 2020; Zhu et al., 2018), which reveals the dominant control of mantle partial melting on the Ca isotope composition of arc magma. Notably, although the source of arc magma is generally more depleted than DMM (e.g., Nebel et al., 2015; Woodhead et al., 1993), the $\delta^{44/40}$Ca difference between arc magmas and MORBs cannot be recognized due to the slightly larger analytical precision (±0.11–0.16 ‰, 2SD for $\delta^{44/40}$Ca) than the fractionation scale caused by partial melting (0–0.1‰).

Interestingly, several lines of evidence reveal carbonate metasomatism occurred in the mantle source of samples in this study. Previous studies found higher δ^{13}C in Central America volcanic gases (−6.8 to −2.7‰, Fig. 5a, Allard, 1983; Sano and Williams, 1996; Shaw et al., 2003) and the Lesser Antilles (−2 to −9‰, Fig. 5a, Van Soest et al., 1998) than the mantle value (−8 to −4‰, Javoy and Pineau, 1991; Cartigny, 2005; Howell et al., 2020). Because carbonate sediments usually have heavier carbon isotope composition (δ^{13}C > −4‰, e.g., Sadofsky and Bebout, 2004; Li and Bebout, 2005; House et al., 2019; Li et al., 2020), such a signature reveals the contribution of carbonate materials. In addition, Southern Lesser Antilles rocks in this study are characterized by a high ^{87}Sr/^{86}Sr ratio (0.705326–0.706373, Fig. 5b), confirming the involvement of recycled sedimentary materials in the source of arc magmas. However, the MORB-like $\delta^{44/40}$Ca, as well as the absence of correlation between $\delta^{44/40}$Ca and δ^{13}C or ^{87}Sr/^{86}Sr (Fig. 5) manifest that the subducted carbonates have a negligible role in fractionating the Ca isotope compositions of arc magmas in this study. Moreover, $\delta^{44/40}$Ca of arc magmas show no correlation with fluid (e.g., Ba/Th and Ba/La) and melt metasomatism indicators (e.g., Sr/Y and Hf/Lu) (Fig. 6), suggesting that whether carbonates transferring via melt or fluid has no difference to influence the Ca isotope budget of arc magmas (see Fig. 6).

5.2. Lack of subducted carbonate Ca isotope signal in arc magmas

Although Ca isotope data of arc magma remain scarce, it seems that most arc magmas have MORB-like Ca isotope

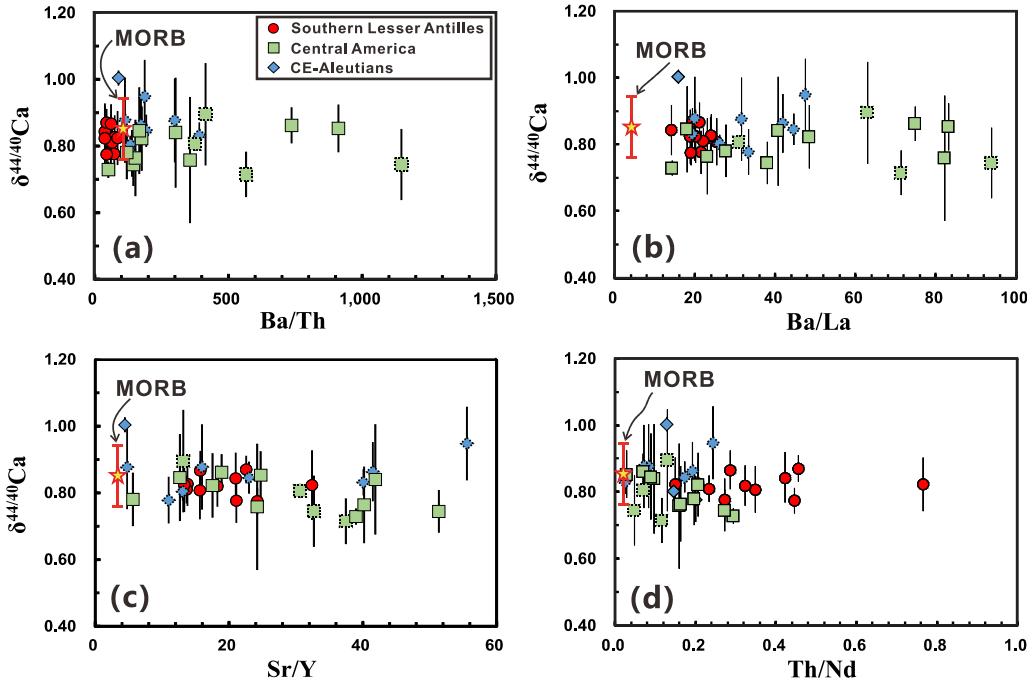

Fig. 6. $\delta^{44/40}$Ca of arc magma versus (a) Ba/Th, (b) Ba/La, (c) Sr/Y, and (d) Th/Nd. The average composition of fresh MORBs (Chen et al., 2020; Zhu et al., 2018) is shown as a star. (For interpretation of the references to colour in this figure legend, the reader is referred to the web version of this article.)

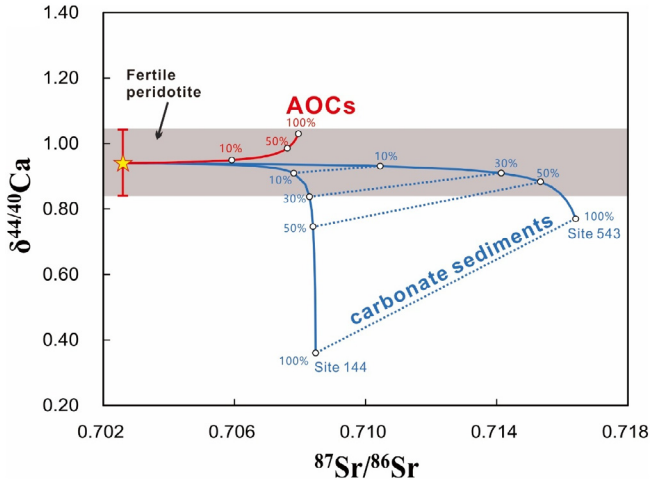

Fig. 7. Mixing model between fertile peridotite with carbonate sediments and with carbonate-bearing AOCs. Compositions of the end members in the modeling are as follows. (1) Mantle: output Ca flux = 3.89×10^{16} kg/Ma (Central America value in Table 2), $\delta^{44/40}Ca = 0.94‰$ (Kang et al., 2017; Chen et al., 2019), Sr content = 9.8 ppm and $^{87}Sr/^{86}Sr = 0.702630$ (Salters and Stracke, 2004); (3) carbonate-bearing AOCs: input Ca flux = 3.98×10^{16} kg/Ma (Central America value in Table 2), $\delta^{44/40}Ca = 1.03‰$ (average value of AOCs reported in Blättler and Higgins, 2017; Chen et al. 2020), Sr content = 144 ppm and $^{87}Sr/^{86}Sr = 0.707954$ (average value of AOCs reported in Hauff et al., 2003); (4) Carbonate sediments: Input Ca flux = 1.95×10^{16} kg/Ma (Central America value in Table 2). Ca isotope, $^{87}Sr/^{86}Sr$ and Sr content are the average value of carbonates from the two sites at the Lesser Antilles forearc (Site 144 and Site 543, Zhu et al., 2020b). Site 144 ($\delta^{44/40}Ca = 0.36‰$, Sr content = 685 ppm and $^{87}Sr/^{86}Sr = 0.70848$). Site 543 ($\delta^{44/40}Ca = 0.77‰$, Sr content = 116 ppm and $^{87}Sr/^{86}Sr = 0.71641$). The gray bar represents the range of fertile peridotite ($0.94 \pm 0.1‰$, Kang et al., 2017; Chen et al., 2019).

composition. For instance, the BABBs from the southwestern Pacific are interpreted to incorporate various amounts of AOC or sediments-derived fluids into their source region, as evidenced by the enriched $^{87}Sr/^{86}Sr$ and $^{143}Nd/^{144}Nd$ ratio (Zhu et al., 2020a). Nevertheless, these samples show $\delta^{44/40}Ca$ of 0.73‰ to 0.89‰, comparable to the samples in this study. In addition, Wang et al. (2021) reported a similar $\delta^{44/40}Ca$ range (~0.84‰) in back-arc basalts from Tonga and Mariana. Combined with new data of the three arcs examined here, of which the sedimentary layer varies from carbonate-rich (Central America) to carbonate-poor (Central-Eastern Aleutians) (Plank, 2014) and thermal regime of subduction zone varies from intermediate (Central America) to cool (Central-Eastern Aleutians) (Syracuse et al., 2010), it appears that subducted carbonates show a minimal effect on modifying the Ca isotope composition of the arc magmas.

The Ca isotope composition of arc magma would be unchanged if subducted carbonate has a similar Ca isotope composition with mantle. A recent study by Blättler and Higgins (2017) found global sedimentary carbonates through much of the Precambrian (3.0–0.54 Ga) have an average $\delta^{44/40}Ca$ similar to the fertile mantle and carbonate veins in AOC from western Pacific (ODP Site 801) have slightly heavier $\delta^{44/40}Ca$ (0.49–1.31‰, with an average value of $1.03 \pm 0.35‰$) than fresh MORB (~0.85‰). As a result, Ionov et al. (2019) suggested that the subducted carbonate may not significantly change the Ca isotope composition of mantle at a global scale. However, $\delta^{44/40}Ca$ of carbonates vary from the mantle value by $\pm$ 0.7‰, which depends on the local mineralogical, precipitation chemistry, and late-stage diagenetic effects (Blättler and Higgins, 2017). As the three arcs in this study have significantly different sediments chemistry (Plank, 2014), it is unlikely that the subducted carbonates from these three arcs have consistent $\delta^{44/40}Ca$ that exactly equals to the mantle value. Most importantly, Zhu et al. (2020b) found the carbonate-rich sediments from Southern Lesser Antilles fore-arc have $\delta^{44/40}Ca \sim 0.6‰$ lower than the mantle value whereas Southern Lesser Antilles arc magmas in this study show MORB-like $\delta^{44/40}Ca$ value. Therefore, the MORB-like $\delta^{44/40}Ca$ in arc magmas should not simply reflect a mantle-like $\delta^{44/40}Ca$ in subducted carbonates.

The Ca isotope signature of arc magma may reflect that little subducted Ca are incorporated into their source. Whether the source of arc magmas experienced Ca enrichment or not can be identified by the CaO content of primary arc magma (Mg# > 60) because its CaO content is less affected by fractional crystallization (Kelemen et al., 2014). As displayed by the data compiled in Kelemen et al. (2014) (see their Fig. 1) and Elliott (2003), global primary arc magmas have CaO content similar to that of primary MORB (Mg# > 60). This suggests that the source of arc magma may not undergo significant Ca enrichment relative to DMM. Several processes may account for this including (i) The high Ca content and different $\delta^{44/40}Ca$ characteristic of subducted carbonate may be well buffered by the mantle wedge before carbonate material reaching the melting zone; (ii) subducted Ca is conveyed to the mantle wedge but being stored as carbonate or Ca-rich silicate minerals; (iii) Ca in carbonate may be retained in the slab and be brought beyond the sub-arc depth.

5.2.1. *The buffering effect of the mantle wedge*

If the amount of Ca in the mantle wedge is much larger than that contributed by the subducted slab, the various

$\delta^{44/40}$Ca of subducted carbonate could be homogenized by isotope exchange with the ambient mantle prior to arriving at the melting zone. To determine whether the Ca flux from carbonate can be buffered by the sub-arc mantle wedge or not, we calculated the Ca input flux of subducted carbonate at Central America and Central-Eastern Aleutians. The model assumes that all the inorganic carbon in the sedimentary layers and oceanic crust are in the form of $CaCO_3$. Considering that a certain amount of carbonate may be $CaMg(CO_3)_2$ or $MgCO_3$, the modeling results should be regarded as an upper limit. More parameters can be found in the supplementary materials. The calcium input flux of sedimentary carbonates was estimated based on the carbon concentration of sediments (Plank, 2014) by deducting the organic carbon with an average ratio of 20 wt.% (Plank and Manning, 2019). The calcium input flux of carbonated oceanic crust is calculated according to the estimation of carbon flux in young AOC by Li et al. (2019). The contribution of the carbonate-bearing serpentinized oceanic mantle is omitted here because serpentinization is only pronounced at slow-spreading ridges and makes a minor contribution to the global input flux (Plank and Manning, 2019). The modeling results are listed in Table 2. Although Central America has the most abundant sedimentary carbonates among global arcs (e.g., Plank, 2014), its Ca input flux from sedimentary carbonates (1.95×10^{16} kg/Ma) is smaller than that of carbonate-bearing oceanic crust (3.98×10^{16} kg/Ma). This coincides with previous estimates that AOC is the dominant reservoir of subducted carbonate (Alt and Teagle, 1999; Dasgupta and Hirschmann, 2010; Jarrard, 2003). As a result, although the Central-Eastern Aleutians arc has no $CaCO_3$ in the sedimentary layer, its total Ca input flux is in the same order of magnitude as that of the Central America arc (5.93×10^{16} kg/Ma for Central America vs. 2.71×10^{16} kg/Ma for Central-Eastern Aleutians, Table 2).

The Ca amount of lithospheric mantle and convective mantle wedge in a region with a typical sub-arc depth of 100 km (e.g., Bebout, 2014; Syracuse and Abers, 2006) are calculated based on the subduction angle (Syracuse et al., 2010), the density of mantle wedge (Savov et al., 2007), the thickness of crust and lithospheric mantle (Carr, 1984; Grevemeyer et al., 2007; Grow, 1973; Shillington et al., 2004), and the width of arc segments (Jarrard, 2003). If assuming that the mantle convection rate is similar to the subduction rate, we calculate that the output Ca flux by mantle convection is 3.89×10^{16} kg/Ma for Central America and 2.62×10^{16} kg/Ma for Central-Eastern Aleutians, respectively. Notably, these results, are in the same order of magnitude as the total Ca input flux from subducted carbonate. Therefore, whether the mantle wedge can buffer the carbonate Ca isotope signal should be controlled by the efficiency of subducted carbonate that can be mobilized into the mantle wedge (referred as carbonate recycling efficiency hereafter).

We employ a Ca-Sr mixing model to determine the Ca isotope budget of the mantle wedge (Fig. 7). The results show that, if the subducted Ca is mainly derived from the carbonate-bearing AOC, the Ca isotope composition of the mantle wedge would be unchanged even if 100% of the subducted carbonate is mobilized into the mantle wedge. This could be the case for the Aleutians subduction zone where carbonates are dominantly stored in AOCs (Plank and Manning, 2019). For subduction zones where abundant sedimentary Ca-rich carbonate subducted, the carbonate Ca isotope signal may not be homogenized if carbonate recycling efficiency is higher than ~30%. However, to our knowledge, the carbonate recycling efficiency has not yet been investigated for arcs of this study. Considering that carbon may be transported together with Ca, and then be degassed as CO_2 through arc volcanoes. The carbon recycling efficiency of subduction zones, defined as the ratio of the recycled carbon flux in volcanic gas to the input flux of subducted carbon, can be used to evaluate the carbonate recycling efficiency. By first order, the subduction zone with high carbon recycling efficiency is potentially associated

Table 2
Part of the parameters used and results calculated for the Ca flux in subduction zones. More parameters can be found in the supplementary materials.

Parameters	Central America	References	Central-Eastern Aleutians	References	Unit
Subduction angle	60	Syracuse et al. (2010)	50	Syracuse et al. (2010)	°
Width of arc segment	1500	Jarrard (2003)	1246	Jarrard (2003)	km
Thickness of crust	40	Carr (1984)	35	Shillington et al. (2004)	km
Thickness of lithospheric mantle	10	Grevemeyer et al. (2007)	45	Grow (1973)	km
Subduction rate	72	Jarrard (2003)	59	Jarrard (2003)	km/Ma
Input Ca flux of sedimentary carbonate	1.95E+16		0		kg/Ma
Input Ca flux of AOCs	3.98E+16		2.71E+16		kg/Ma
Total input Ca flux from slab	5.93E+16		2.71E+16		kg/Ma
Ca mass of lithospheric mantle	3.37E+16		1.20E+17		kg
Ca mass of convective mantle	5.26E+16		1.02E+16		kg
Output Ca flux by mantle convection	3.89E+16		2.62E+16		kg/Ma

with efficient mobilization of carbonate into the mantle wedge.

The carbon recycling efficiency of the arc segment is controlled by several physical parameters such as sediments type and thermal structure of subduction zone (e.g., Kerrick and Connolly, 2001). The arcs investigated in this study vary greatly from low efficiency (0.1% for Aleutians and 14–21% for Central America, Johnston et al., 2011; Shaw et al., 2003) to high efficiency of >70% for the Lesser Antilles (Johnston et al, 2011; Li et al., 2020). Therefore, the MORB-like Ca isotope composition of Aleutians and Central American rocks can be explained by the buffering effect of the mantle wedge. But for the Lesser Antilles, the mantle wedge may not be capable of homogenizing the variable subducted Ca isotope of carbonate and other mechanisms should be taken into account.

5.2.2. Subducted Ca storage in the mantle wedge or arc crust

Calcium in carbonate may not be incorporated into arc magma if the mobilized Ca is re-precipitated as carbonates or silicate minerals in the mantle wedge or crust (Kelemen and Manning, 2015). The solubility of $CaCO_3$ in fluids at sub-arc depth can reach up to ~5000 ppm (Kelemen and Manning, 2015), which suggests that large amounts of calcium carbonates in the overlying oceanic crust and sedimentary layers could be dissolved in the fluid expelled from serpentinized slab mantle. This is also supported by the 1:1 CO_2: Ca (molar ratio) losses caused by fluid infiltration in the marble-bearing subduction complex rocks (Ague and Nicolescu, 2014). However, the solubility of carbonate will be dramatically decreased due to the cooling and decompression as fluid transits through the mantle wedge (Kelemen and Manning, 2015). Large amounts of dissolved $CaCO_3$ can thus be re-precipitated and stored in the mantle wedge or crust (Kelemen and Manning, 2015). For example, Ducea et al. (2005) found calcite globules and veins occurred in the sub-Sierra Nevada peridotite xenoliths, which represent a slice of lithospheric mantle wedge beneath the Mesozoic California magmatic arc. In addition, the extensive occurrence of calcite veining throughout the Central America fore-arc suggests that some of the subducted carbon can be sequestered into the crust as calcite (Barry et al., 2019; Corrigan et al., 1990; Vaca et al., 1989). These deposited calcites could be a hidden reservoir for subducted Ca and thus explains why the two fore-arc volcanics from Central America have MORB-like Ca isotope composition. On the other hand, the re-precipitation of calcite may fractionate the Ca isotope composition of residue fluid towards a heavier value (John et al., 2012). However, no heavy Ca isotope signature is observed in arc magmas, possibly reflecting the low Ca content in the residual fluid after significant calcite re-precipitation.

In addition to fluid-induced dissolution, considerable amounts of subducted carbonates can be transported into the mantle wedge by buoyant diapirs owing to the low density and low viscosity of the sedimentary layers (e.g., Behn et al., 2011; Kelemen et al., 2011). When the sedimentary diapiric flow passes through the hot core of the mantle wedge, carbonates may undergo high degrees of partial melting and mostly are transferred into carbonate-bearing silicate melts (Kelemen and Manning, 2015). When such melts rise into the lithosphere and lower crust <1250 °C, the melts will encounter the shelf in the carbonated peridotite solidus (Kelemen and Manning, 2015). CO_2-rich fluid + olivine + pyroxene + garnet or spinel become more stable with respect to carbonate-bearing silicate melt. As a result, subducted Ca could be stored in the mantle wedge or crust as Ca-rich silicates rather than being recycled to the surface through arc volcanoes. But it should be noticed that few studies investigate the diapiric rising of meta-sediments in mantle wedge (Kelemen et al., 2014; Behn et al., 2011). The fate of sedimentary diapirs in the subduction zone remains speculative.

5.2.3. Calcium retaining on the descending slab

The MORB-like Ca isotope composition in arc magma may alternatively reflect the retention of subducted Ca beyond the sub-arc depth. Metamorphic decarbonation reaction (e.g., $SiO_2 + CaCO_3 = CaSiO_3 + CO_2$) can break down carbonate and release CO_2 at the subduction zone (e.g., Galvez et al., 2013; Kerrick and Connolly, 2001) while incorporating Ca into silicate mineral (e.g., wollastonite) in the subducted slab. A recent study by Lu et al. (2019) found that the Ca content and $\delta^{44/40}Ca$ of meta-basaltic rocks from the Dabie-Sulu orogen are unchanged during prograde metamorphism. Therefore, the Ca in carbonate could retain in the slab as silicate minerals rather than be released to the overlying mantle wedge. But it should be emphasized that recent experimental and modeling studies revealed that significant decarbonation is practical only at low pressure and hot subduction zones (Molina and Poli, 2000). Most of the subducted carbonates hence may not undergo metamorphic decarbonation reaction.

Isotope exchange between eclogite and carbonate is also possible to fix subducted Ca on the slab. Wang et al. (2014) found that the eclogites from Dabie-Sulu regions show extremely heavy $\delta^{18}O$ (up to 21.1‰) and light $\delta^{26}Mg$ (down to −1.928‰ in garnet) compared with the protoliths. The associated ultrahigh-pressure metamorphic (UHPM) marbles show a negative correlation between $\delta^{26}Mg$ (from −2.508 to −0.531‰) and MgO/CaO ratio. These signatures reflect the extensive Mg isotope exchange between eclogite and carbonate driven by prograde metamorphism. Similarly, Ca isotope exchange between carbonate and eclogite is also possible to occur and will convey the Ca isotope signal of carbonate to the descending slab.

Furthermore, regarding arcs with low carbonate recycling efficiency, a large number of carbonates may survive fluid-dissolution, diapirism rising and metamorphic decarbonation (e.g., Connolly, 2005; Gorman et al., 2006; Dasgupta and Hirschmann, 2010; Plank and Manning, 2019). For example, abundant carbonate mineral inclusions (calcite, dolomite, and magnesite) were found in the metasomatized zircons from the ultra-mafic massif of Dabie orogeny (Shen et al., 2018), suggesting that the subducted carbonate could be transferred beyond sub-arc depth (>100 km).

5.3. Implications for Ca and carbonate recycling in subduction zones

Simplified scenarios for Ca and carbonate cycling in subduction zone can be outlined (Fig. 8): 1) at subduction zones with low carbonate recycling efficiency (<30%) or subducted Ca mainly in the form of carbonate-bearing AOCs (e.g., Aleutians and Central America), the buffering effect of mantle wedge alone can explain the MORB-like Ca isotope composition in arc magmas; 2) at subduction zones with high carbonate recycling efficiency (>30%, e.g., the Lesser Antilles in this study), most carbonate could be mobilized into the mantle wedge. A number of factors could simultaneously contribute to the MORB-like Ca isotope in arc magmas, including mantle buffering effect, dissolution-reprecipitation, melting-recrystallization, metamorphic decarbonation, and carbonate-eclogite isotope exchange. The first three processes would store subducted Ca in mantle wedge while the latter two processes fix subducted Ca on the descending slab. Notably, the mantle wedge peridotite is static at shallow depths, but will be coupled to the descent slab at a certain deep depth because of the decreasing viscosity and strength (e.g., van Keken et al., 2011). Therefore, part of the subducted Ca that preserved in the mantle wedge may be gradually dragged downwards into the deeper mantle (Plank and Manning, 2019). Overall, along with the Ca retaining on the slab, most subducted Ca may be carried into the deep mantle. This is further supported by the carbonate Ca isotope signals that have been observed in OIB and intra-plate igneous rocks, such as Hawaii basalts (0.75–1.02‰, Huang et al., 2011b), calc-alkaline basalts from the Southeastern Tibetan Plateau (0.65–0.80‰, Liu et al., 2017a), refractory peridotite xenoliths from the central Siberian craton (0.25–0.96‰, Kang et al., 2017), and peridotite xenoliths from eastern China (0.76–1.17‰, Kang et al., 2016; Chen et al., 2018).

5.4. Comparison with Mg isotope of arc magmas

Magnesium is another metal stable isotope that has shown great potential as a sensitive tracer of deep carbon recycling because carbonates have significantly lighter Mg isotope compositions than BSE (e.g., Teng, 2017). Similar to Ca isotope, carbonate-recycling related low δ^{26}Mg signature has not been observed in arc magmas and sub-arc mantle xenoliths (Teng et al., 2016; Li et al., 2017; Hu et al., 2020) but frequently found in intra-plate igneous rocks (e.g., Yang et al., 2012; Huang et al., 2015; Li et al., 2017) and OIBs (e.g., Wang et al., 2018). This is attributed to the low solubility of dolomite and magnesite at sub-arc depth based on the result of molecular dynamics (Pan et al., 2013; Li et al., 2017). But differently, arc lavas from Martinique Island of the Lesser Antilles show heavier Mg isotope compositions (up to 0.06 ± 0.04‰) than samples from Kamchatka and Central America (about −0.24‰). Because altered abyssal peridotites and constituent phyllosilicates often have heavy Mg isotope compositions (e.g., Liu et al., 2017c), the heavy Mg isotope compositions in arc magmas can be explained by the incorporation of fluids expelled from the subducted slab mantle (Teng et al., 2016).

However, this effect is not observed for Ca isotope compositions of Kick'em-Jenny lavas from the Lesser Antilles arc. Notably, Kick'em-Jenny lavas have higher $^{87}Sr/^{86}Sr$ ratios (0.7053–0.7063) than lavas from Martinique Island (~0.7035, Teng et al., 2016), indicating the subducted materials is sedimentary rather than peridotitic. In addition, the Ba/Th ratios of Kick 'em-Jenny lavas (38–85) are lower

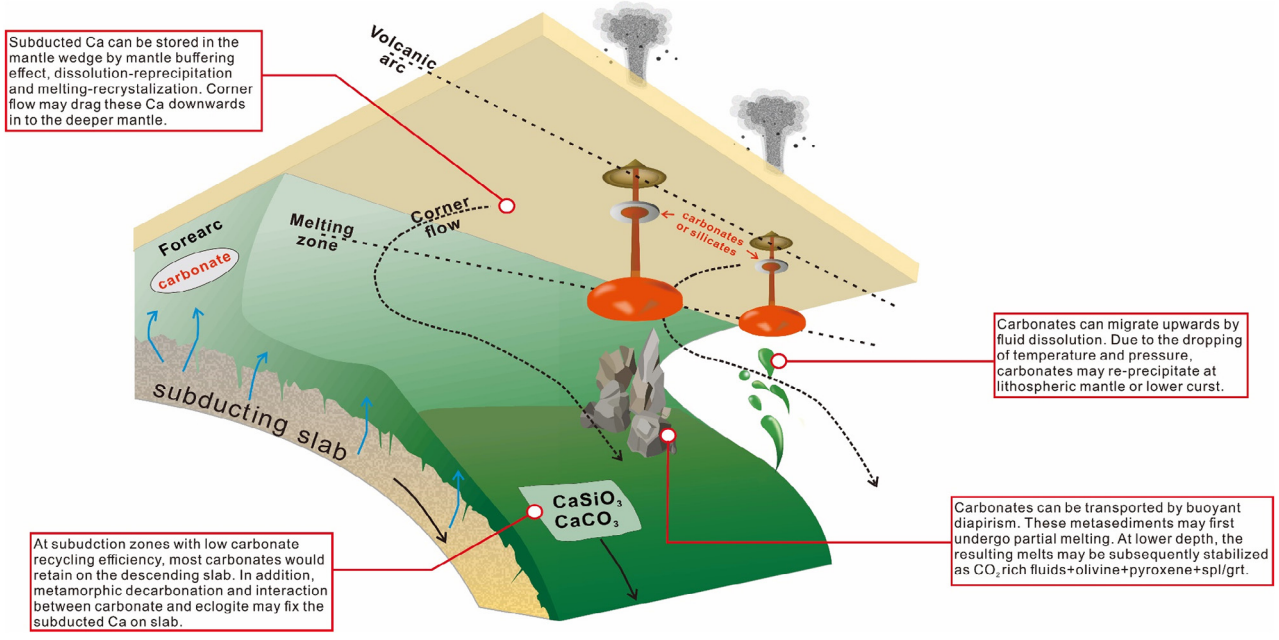

Fig. 8. Schematic illustration of subducted Ca and carbonate recycling in a subduction zone (modified after Marschall and Schumacher, 2012). More descriptions can be found in the main text.

than that of Martinique rocks (37.1–133.5), which further precludes the infiltration by large amounts of fluids dehydrated from slab mantle. On the other hand, the Ca isotope composition of altered abyssal peridotite has not yet been investigated. It is still not clear whether fluids released from the slab mantle can modify the Ca isotope composition of the overlying mantle wedge or not.

6. CONCLUSIONS

Arc magmas from Central America, Central Eastern Aleutian, and Southern Lesser Antilles have an average $\delta^{44/40}$Ca of 0.82 ± 0.12‰ (2SD, n = 36), which is lighter than the fertile peridotite and is comparable to the reported values of fresh MORBs. The $\delta^{44/40}$Ca of these rocks show no correlation with indices of post-magmatic alteration (CIA and Rb/TiO_2), crustal contamination (Ti/Zr and Nb/La), and magma evolution (SiO_2, CaO, MgO and Eu/Eu*). Most importantly, the $\delta^{44/40}$Ca of arc magmas show no cross-arc variations and do not correlate with Ba/La, Ba/Th, Sr/Y, Th/Nd, and $^{87}Sr/^{86}Sr$, suggesting that the varied Ca isotope compositions in subducted carbonates is not embodied in arc magmas. Therefore, the Ca isotope offset between arc magmas and fertile peridotite should reflect the fractionation during mantle partial melting. The Ca input flux of subducted carbonate was calculated to assess whether the MORB-like Ca isotope composition of arc magmas reflect the buffering effect of mantle wedge or not. Our results suggest that the buffering effect can explain if carbonate recycling efficiency is lower than 30% or the subducted carbonates are mainly in the form of carbonate-bearing AOCs. For subduction zones with carbonate recycling efficiency higher than 30%, it may also reflect the storage of subducted Ca in the mantle wedge and the retention of subducted Ca in the descending slab beyond sub-arc depth. Combined with the fact that carbonate Ca isotope signal is frequently observed in intra-plate igneous rocks, we infer that most subducted Ca may finally enter the deep mantle and return to the surface through oceanic basalt and intra-plate igneous rocks.

Declaration of Competing Interest

The authors declare that they have no known competing financial interests or personal relationships that could have appeared to influence the work reported in this paper.

ACKNOWLEDGMENTS

We thank Dr. Ariel Anbar and the W. M. Keck Foundation Laboratory for Environmental Biogeochemistry at ASU for providing instrumentation and laboratory facility for Ca isotope measurement. We thank Stephen Romaniello, Gwyneth Gordon, and Fang Liu for the assistance with isotope analysis. We gratefully thank Yue Cai, Gerhard Wörner and Haraldur Sigurdsson for providing precious samples. The discussion with Jian Huang and Hongli Zhu is greatly appreciated. Maryjo Brounce, Elsa Amsellem and an anonymous referee are gratefully acknowledged for their constructive reviews, as is Shichun Huang for his thorough editorial handling. This work is financially supported by the National Key R&D Program of China (Grant No. 2019YFA0708400), Strategic Priority Research Program (B) of Chinese Academy of Sciences (Grant No. XDB410000000), pre-research Project on Civil Aerospace Technologies funded by Chinese National Space Administration (Grant No. D020202), and the National Natural Science Foundation of China (Grant No. 41903002, 41873002, 41630206, 41571130052, 41325011).

APPENDIX A. SUPPLEMENTARY MATERIAL

Supplementary data to this article can be found online at https://doi.org/10.1016/j.gca.2021.05.014.

REFERENCES

Abratis M and Wörner G (2001) Ridge collision, slab-window formation, and the flux of Pacific asthenosphere into the Caribbean realm. *Geol.* **29**(2), 127–130.

Ague J. J. and Nicolescu S. (2014) Carbon dioxide released from subduction zones by fluid-mediated reactions. *Nat. Geosci.* **7**, 355–360.

Albarède F. and Beard B. (2004) Analytical methods for non-traditional isotopes. *Rev. Mineral. Geochem.* **55**, 113–152.

Allard P. (1983) The origin of hydrogen, carbon, sulphur, nitrogen and rare gases in volcanic exhalations: evidence from isotope geochemistry. In *Forecasting volcanic events*. Elsevier, pp. 337–386.

Alt J. and Teagle D. (1999) The uptake of carbon during alteration of ocean crust. *Geochim. Cosmochim. Acta* **63**, 1527–1535.

Amsellem E., Moynier F., Bertrand H., Bouyon A., Mata J., Tappe S. and Day J. M. D. (2020) Calcium isotopic evidence for the mantle sources of carbonatites. *Sci. Adv.* **6**, 23.

Amsellem E., Moynier F., Pringle E. A., Bouvier A., Chen H., Day J. and Letters P. S. (2017) Testing the chondrule-rich accretion model for planetary embryos using calcium isotopes. *Earth Planet. Sci. Lett.* **469**, 75–83.

Amsellem E., Moynier F. and Puchtel I. S. (2019) Evolution of the Ca isotopic composition of the mantle. *Geochim. Cosmochim. Acta* **258**, 195–206.

Banerjee A. and Chakrabarti R. (2019) A geochemical and Nd, Sr and stable Ca isotopic study of carbonatites and associated silicate rocks from the ~65 Ma old Ambadongar carbonatite complex and the Phenai Mata igneous complex, Gujarat, India: Implications for crustal contamination, carbonate recycling, hydrothermal alteration and source-mantle mineralogy. *Lithos*, 572–585.

Barry P. H., de Moor J. M., Giovannelli D., Schrenk M., Hummer D. R., Lopez T., Pratt C. A., Segura Y. A., Battaglia A., Beaudry P., Bini G., Cascante M., d'Errico G., di Carlo M., Fattorini D., Fullerton K., Gazel E., Gonzalez G., Halldorsson S. A., Iacovino K., Ilanko T., Kulongoski J. T., Manini E., Martinez M., Miller H., Nakagawa M., Ono S., Patwardhan S., Ramirez C. J., Regoli F., Smedile F., Turner S., Vetriani C., Yucel M., Ballentine C. J., Fischer T. P., Hilton D. R. and Lloyd K. G. (2019) Forearc carbon sink reduces long-term volatile recycling into the mantle. *Nature* **568**, 487–492.

Bebout, G. (2014) 4.20 - Chemical and Isotopic Cycling in Subduction Zones, pp. 703–747.

Behn M. D., Kelemen P. B., Hirth G., Hacker B. R. and Massonne H.-J. (2011) Diapirs as the source of the sediment signature in arc lavas. *Nat. Geosci.* **4**, 641–646.

Blättler C. L. and Higgins J. A. (2017) Testing Urey's carbonate–silicate cycle using the calcium isotopic composition of sedimentary carbonates. *Earth Planet. Sci. Lett.* **479**, 241–251.

Burnham A., Thomson A., Bulanova G., Smith C., Walter M. and Kohn S. (2015) Stable isotope evidence for crustal recycling as recorded by superdeep diamonds. *Earth Planet. Sci. Lett.* **432**, 374–380.

Cai Y., LaGatta A., Goldstein S. L., Langmuir C. H., Gómez-Tuena A., Martín-del Pozzo A. L. and Carrasco-Núñez G. (2014) Hafnium isotope evidence for slab melt contributions in the Central Mexican Volcanic Belt and implications for slab melting in hot and cold slab arcs. *Chem. Geol.* **377**, 45–55.

Cai Y., Rioux M., Kelemen P. B., Goldstein S. L., Bolge L. and Kylander-Clark A. R. (2015) Distinctly different parental magmas for calc-alkaline plutons and tholeiitic lavas in the central and eastern Aleutian arc. *Earth Planet. Sci. Lett.* **431**, 119–126.

Carr M. J. (1984) Symmetrical and segmented variation of physical and geochemical characteristics of the Central American volcanic front. *J. Volcanol. Geoth. Res.* **20**, 231–252.

Cartigny P. (2005) Stable isotopes and the origin of diamond. *Elements* **1**, 79–84.

Chen C., Ciazela J., Li W., Dai W., Wang Z., Foley S. F., Li M., Hu Z. and Liu Y. (2020) Calcium isotopic compositions of oceanic crust at various spreading rates. *Geochim. Cosmochim. Acta* **278**, 272–288.

Chen C., Dai W., Wang Z., Liu Y., Li M., Becker H. and Foley S. F. (2019) Calcium isotope fractionation during magmatic processes in the upper mantle. *Geochim. Cosmochim. Acta* **249**, 121–137.

Chen C., Liu Y., Feng L., Foley S. F., Zhou L., Ducea M. N. and Hu Z. (2018) Calcium isotope evidence for subduction-enriched lithospheric mantle under the northern North China Craton. *Geochim. Cosmochim. Acta* **238**, 55–67.

Clift P. D. (2017) A revised budget for Cenozoic sedimentary carbon subduction. *Rev. Geophys.* **55**, 97–125.

Connolly J. (2005) Computation of phase equilibria by linear programming: A tool for geodynamic modeling and an application to subduction zone decarbonation. *Earth Planet. Sci. Lett.* **236**, 524–541.

Corrigan J. D., Mann P. and Ingle J. C. (1990) Forearc response to subduction of the Cocos Ridge, Panama-Costa Rica. *Geol. Soc. Am. Bull.* **102**, 628–652.

Dasgupta R. and Hirschmann M. M. (2010) The deep carbon cycle and melting in Earth's interior. *Earth Planet. Sci. Lett.* **298**, 1–13.

Dasgupta R., Mallik A., Tsuno K., Withers A., Hirth G. and Hirschmann M. (2013) Carbon-dioxide-rich silicate melt in the Earth's upper mantle. *Nature* **493**, 211–215.

de Boer J. Z., Defant M., Stewart R., Restrepo J., Clark L. and Ramirez A. (1988) Quaternary calc-alkaline volcanism in western Panama: regional variation and implication for the plate tectonic framework. *J. S. Am. Earth Sci.* **1**, 275–293.

Devine J. D. (1995) Petrogenesis of the basalt-andesite-dacite association of Grenada, Lesser Antilles island arc, revisited. *J. Volcanol. Geoth. Res.* **69**, 1–33.

Devine J. D. and Sigurdsson H. (1995) Petrology and eruption styles of Kick'em-Jenny submarine volcano, Lesser Antilles island arc. *J. Volcanol. Geoth. Res.* **69**, 35–58.

Drummond M. S. and Defant M. J. (1990) A model for Trondhjemite-Tonalite-Dacite Genesis and crustal growth via slab melting: Archean to modern comparisons. *J. Geophys. Res.* **95**, 21503–21521.

Ducea M. N., Saleeby J., Morrison J. and Valencia V. A. (2005) Subducted carbonates, metasomatism of mantle wedges, and possible connections to diamond formation: An example from California. *Am. Mineral.* **90**, 864–870.

Elliott T. (2003) Tracers of the slab. *Geophysical Monograph-American Geophysical Union* **138**, 23–46.

Fantle M. S. and Tipper E. T. (2014) Calcium isotopes in the global biogeochemical Ca cycle: Implications for development of a Ca isotope proxy. *Earth-Sci. Rev.* **129**, 148–177.

Feng L. P., Zhou L., Yang L., DePaolo D. J., Tong S. Y., Liu Y. S., Owens T. L. and Gao S. (2017) Calcium isotopic compositions of sixteen USGS reference materials. *Geostand. Geoanal. Res.* **41**, 93–106.

Foley S. (2010) A reappraisal of redox melting in the earth's mantle as a function of tectonic setting and time. *J. Petrol.* **52**, 1363–1391.

Frezzotti M. L., Selverstone J., Sharp Z. D. and Compagnoni R. (2011) Carbonate dissolution during subduction revealed by diamond-bearing rocks from the Alps. *Nat. Geosci.* **4**, 703–706.

Galvez M., Beyssac O., Martinez I., Benzerara K., Chaduteau C., Malvoisin B. and Malavieille J. (2013) Graphite formation by carbonate reduction during subduction. *Nat. Geosci.* **6**, 473–477.

Gorman P. J., Kerrick D. M. and Connolly J. A. D. (2006) Modeling open system metamorphic decarbonation of subducting slabs. *Geochem. Geophys. Geosyst.* **7**, 2006.

Grevemeyer I., Ranero C. R., Flueh E. R., Kläschen D. and Bialas J. (2007) Passive and active seismological study of bending-related faulting and mantle serpentinization at the Middle America trench. *Earth Planet. Sci. Lett.* **258**, 528–542.

Grow J. A. (1973) Crustal and upper mantle structure of the Central Aleutian Arc. *Geol. Soc. Am. Bull.* **84**, 2169–2192.

Hauff F., Hoernle K. and Schmidt A. (2003) Sr-Nd-Pb composition of Mesozoic Pacific oceanic crust (Site 1149 and 801, ODP Leg 185): Implications for alteration of ocean crust and the input into the Izu-Bonin-Mariana subduction system. *Geochem. Geophys. Geosyst.* **4**.

Hawkesworth C., Turner S., Peate D., McDermott F. and van Calsteren P. (1997) Elemental U and Th variations in island arc rocks: implications for U-series isotopes. *Chem. Geol.* **139**, 207–221.

Heath E., Turner S. P., Macdonald R., Hawkesworth C. J. and Van Calsteren P. (1998) Long magma residence times at an island arc volcano (Soufriere, St. Vincent) in the Lesser Antilles: evidence from 238U–230Th isochron dating. *Earth Planet. Sci. Lett.* **160**, 49–63.

Herrstrom E., Reagan M. K. and Morris J. D. (1995) Variations in lava composition associated with flow of asthenosphere beneath southern Central America. *Geology* **23**, 617–620.

Heuser A., Eisenhauer A., Gussone N., Bock B., Hansen B. and Nägler T. F. (2002) Measurement of calcium isotopes (δ44Ca) using a multicollector TIMS technique. *Int. J. Mass Spect.* **220**, 385–397.

Hilton D., Fischer T. and Marty B. (2002) Noble gases and volatile recycling at subduction zones. *Rev. Mineral. Geochem.* **47**, 319–370.

House B. M., Bebout G. E. and Hilton D. R. (2019) Carbon cycling at the Sunda margin, Indonesia: A regional study with global implications. *Geology* **47**, 483–486.

Howell D., Stachel T., Stern R. A., Pearson D. G., Nestola F., Hardman M. F., Harris J. W., Jaques A. L., Shirey S. B., Cartigny P., Smit K. V., Aulbach S., Brenker F. E., Jacob D. E., Thomassot E., Walter M. J. and Navon O. (2020) Deep carbon through time: Earth's diamond record and its implications for carbon cycling and fluid speciation in the mantle. *Geochim. Cosmochim. Acta* **275**, 99–122.

Hu Y., Teng F.-Z. and Ionov D. A. (2020) Magnesium isotopic composition of metasomatized upper sub-arc mantle and its implications to Mg cycling in subduction zones. *Geochim. Cosmochim. Acta* **278**, 219–234.

Huang F. and Lundstrom C. C. (2007) 231Pa excesses in arc volcanic rocks: constraint on melting rates at convergent margins. *Geology* **35**, 1007–1010.

Huang F., Lundstrom C. C., Sigurdsson H. and Zhang Z. (2011a) U-series disequilibria in Kick'em Jenny submarine volcano lavas: A new view of time-scales of magmatism in convergent margins. *Geochim. Cosmochim. Acta* **75**, 195–212.

Huang J., Li S.-G., Xiao Y., Ke S., Li W.-Y. and Tian Y. (2015) Origin of low δ26Mg Cenozoic basalts from South China Block and their geodynamic implications. *Geochim. Cosmochim. Acta* **164**, 298–317.

Huang J., Zhang X.-C., Chen S., Tang L., Wörner G., Yu H. and Huang F. (2018) Zinc isotopic systematics of Kamchatka-Aleutian arc magmas controlled by mantle melting. *Geochim. Cosmochim. Acta* **238**, 85–101.

Huang S., Farkaš J. and Jacobsen S. B. (2010) Calcium isotopic fractionation between clinopyroxene and orthopyroxene from mantle peridotites. *Earth Planet. Sci. Lett.* **292**, 337–344.

Huang S., Farkaš J. and Jacobsen S. B. (2011b) Stable calcium isotopic compositions of Hawaiian shield lavas: evidence for recycling of ancient marine carbonates into the mantle. *Geochim. Cosmochim. Acta* **75**, 4987–4997.

Huang F., Zhou C., Wang W., Kang J. and Wu Z. (2019) First-principles calculations of equilibrium Ca isotope fractionation: Implications for oldhamite formation and evolution of lunar magma ocean. *Earth Planet. Sci. Lett.* **510**, 153–160.

Ionov D. A., Qi Y.-H., Kang J.-T., Golovin A. V., Oleinikov O. B., Zheng W., Anbar A. D., Zhang Z.-F. and Huang F. (2019) Calcium isotopic signatures of carbonatite and silicate metasomatism, melt percolation and crustal recycling in the lithospheric mantle. *Geochim. Cosmochim. Acta* **248**, 1–13.

Jacobson A. D., Grace Andrews M., Lehn G. O. and Holmden C. (2015) Silicate versus carbonate weathering in Iceland: New insights from Ca isotopes. *Earth Planet. Sci. Lett.* **416**, 132–142.

Jarrard R. (2003) Subduction fluxes of water, carbon dioxide, chlorine, and potassium. *Geochem. Geophys. Geosyst.* **4**, 8905.

Jarrard R. D. (1986) Relations among subduction parameters. *Rev. Geophys.* **24**, 217–284.

Javoy M. and Pineau F. (1991) The volatiles record of a "popping" rock from the Mid-Atlantic Ridge at 14 N: chemical and isotopic composition of gas trapped in the vesicles. *Earth Planet. Sci. Lett.* **107**, 598–611.

John T., Gussone N., Podladchikov Y. Y., Bebout G. E., Dohmen R., Halama R., Klemd R., Magna T. and Seitz H.-M. (2012) Volcanic arcs fed by rapid pulsed fluid flow through subducting slabs. *Nat. Geosci.* **5**, 489.

Johnston F., Turchyn A. V. and Edmonds M. (2011) Decarbonation efficiency in subduction zones: Implications for warm Cretaceous climates. *Earth Planet. Sci. Lett.* **303**, 143–152.

Kang J.-T., Ionov D. A., Liu F., Zhang C.-L., Golovin A. V., Qin L.-P., Zhang Z.-F. and Huang F. (2017) Calcium isotopic fractionation in mantle peridotites by melting and metasomatism and Ca isotope composition of the Bulk Silicate Earth. *Earth Planet. Sci. Lett.* **474**, 128–137.

Kang J.-T., Ionov D. A., Zhu H.-L., Liu F., Zhang Z.-F., Liu Z. and Huang F. (2019) Calcium isotope sources and fractionation during melt-rock interaction in the lithospheric mantle: Evidence from pyroxenites, wehrlites, and eclogites. *Chem. Geol.* **524**, 272–282.

Kang J.-T., Zhou C., Huang J.-Y., Hao Y.-T., Liu F., Zhu H.-L., Zhang Z.-F. and Huang F. (2020) Diffusion-driven Ca-Fe isotope fractionations in the upper mantle: Implications for mantle cooling and melt infiltration. *Geochim. Cosmochim. Acta* **290**, 41–58.

Kang J.-T., Zhu H.-L., Liu Y.-F., Liu F., Wu F., Hao Y.-T., Zhi X.-C., Zhang Z.-F. and Huang F. (2016) Calcium isotopic composition of mantle xenoliths and minerals from Eastern China. *Geochim. Cosmochim. Acta* **174**, 335–344.

Kay S. M., Kay R. W., Brueckner H. K. and Rubenstone J. L. (1983) Tholeiitic Aleutian arc plutonism: The Finger Bay pluton, Adak, Alaska. *Contrib. Miner. Petrol.* **82**, 99–116.

Kelemen P. B., Hanghøj K. and Greene A. R. (2014) 4.21 - One View of the Geochemistry of Subduction-Related Magmatic Arcs, with an Emphasis on Primitive Andesite and Lower Crust. In *Treatise on Geochemistry (Second Edition)* (eds. H. D. Holland and K. K. Turekian). Elsevier, Oxford, pp. 749–806.

Kelemen P. B. and Manning C. E. (2015) Reevaluating carbon fluxes in subduction zones, what goes down, mostly comes up. *Proc. Natl. Acad. Sci.* **112**, E3997–E4006.

Kelemen P. B., Matter J., Streit E. E., Rudge J. F., Curry W. B. and Blusztajn J. (2011) Rates and mechanisms of mineral carbonation in peridotite: natural processes and recipes for enhanced, in situ CO_2 Capture and storage. *Annu. Rev. Earth Planet. Sci.* **39**, 545–576.

Kerrick D. M. and Connolly J. (2001) Metamorphic devolatilization of subducted marine sediments and the transport of volatiles into the Earth's mantle. *Nature* **411**, 293–296.

Li K., Li L., Aubaud C. and Muehlenbachs K. (2020) Efficient carbon recycling at the Central-Northern Lesser Antilles Arc: implications to deep carbon recycling in global subduction zones. *Geophys. Res. Lett.* **47**, e2020GL086950.

Li K., Li L., Pearson D. G. and Stachel T. (2019) Diamond isotope compositions indicate altered igneous oceanic crust dominates deep carbon recycling. *Earth Planet. Sci. Lett.* **516**, 190–201.

Li L. and Bebout G. E. (2005) Carbon and nitrogen geochemistry of sediments in the Central American convergent margin: insights regarding subduction input fluxes, diagenesis, and paleoproductivity. *J. Geophys. Res. Solid Earth* **110**, B11202.

Li S.-G., Yang W., Ke S., Meng X., Tian H., Xu L., He Y., Huang J., Wang X.-C. and Xia Q. (2017) Deep carbon cycles constrained by a large-scale mantle Mg isotope anomaly in eastern China. *Natl. Sci. Rev.* **4**, 111–120.

Liu F., Li X., An Y. J., Li J. and Zhang Z. F. (2019a) Calcium Isotope Ratio (δ44/40Ca) Measurements of Ca-Dominated Minerals and Rocks without Column Chemistry Using the Double-Spike Technique and Thermal Ionisation Mass Spectrometry. *Geostand. Geoanal. Res.* **43**, 509–517.

Liu F., Li X., Wang G., Liu Y., Zhu H., Kang J., Huang F., Sun W., Xia X. and Zhang Z. (2017a) Marine carbonate component in the mantle beneath the southeastern Tibetan Plateau: evidence from magnesium and calcium isotopes. *J. Geophys. Res. Solid Earth*, 9729–9744.

Liu F., Zhu H. L., Li X., Wang G. Q. and Zhang Z. F. (2017b) Calcium isotopic fractionation and compositions of geochemical reference materials. *Geostand. Geoanal. Res.* **41**, 675–688.

Liu P.-P., Teng F.-Z., Dick H. J. B., Zhou M.-F. and Chung S.-L. (2017c) Magnesium isotopic composition of the oceanic mantle and oceanic Mg cycling. *Geochim. Cosmochim. Acta* **206**, 151–165.

Liu Y., Chen C., He D. and Chen W. (2019b) Deep carbon cycle in subduction zones. *Sci. China Earth Sci.* **62**, 1764–1782.

Lu W.-N., He Y., Wang Y. and Ke S. (2019) Behavior of calcium isotopes during continental subduction recorded in meta-basaltic rocks. *Geochim. Cosmochim. Acta* **278**, 392–404.

Macdonald R., Hawkesworth C. and Heath E. (2000) The Lesser Antilles volcanic chain: a study in arc magmatism. *Earth-Sci. Rev.* **49**, 1–76.

Marschall H. R. and Schumacher J. C. (2012) Arc magmas sourced from mélange diapirs in subduction zones. *Nat. Geosci.* **5**, 862–867.

Mason E., Edmonds M. and Turchyn A. V. (2017) Remobilization of crustal carbon may dominate volcanic arc emissions. *Science* **357**, 290–294.

Molina J. F. and Poli S. (2000) Carbonate stability and fluid composition in subducted oceanic crust: an experimental study on H_2O–CO_2-bearing basalts. *Earth Planet. Sci. Lett.* **176**, 295–310.

Nebel O., Sossi P., Benard A., Wille M., Vroon P. and Arculus R. (2015) Redox-variability and controls in subduction zones from an iron-isotope perspective. *Earth Planet. Sci. Lett.* **432**, 142–151.

Nesbitt H. and Young G. (1982) Early Proterozoic climates and plate motions inferred from major element chemistry of lutites. *Nature* **299**, 715–717.

Pan D., Spanu L., Harrison B., Sverjensky D. A. and Galli G. A. (2013) Dielectric properties of water under extreme conditions and transport of carbonates in the deep Earth. *PNAS* **110**, 6646–6650.

Pickering-Witter J. and Johnston A. (2000) The effects of variable bulk composition on the melting systematics of fertile peridotitic assemblages. *Contrib. Miner. Petrol.* **140**, 190–211.

Plank T. (2014) 4.17 - The chemical composition of subducting sediments. In *Treatise on Geochemistry (Second Edition)* (eds. H. D. Holland and K. K. Turekian). Elsevier, Oxford, pp. 607–629.

Plank T. and Langmuir C. H. (1998) The chemical composition of subducting sediment and its consequences for the crust and mantle. *Chem. Geol.* **145**, 325–394.

Plank T. and Manning C. E. (2019) Subducting carbon. *Nature* **574**, 343–352.

Romaniello S., Field M., Smith H., Gordon G., Kim M. and Anbar A. (2015) Fully automated chromatographic purification of Sr and Ca for isotopic analysis. *J. Anal. At. Spectrom.* **30**, 1906–1912.

Sadofsky S. J. and Bebout G. E. (2004) Nitrogen geochemistry of subducting sediments: New results from the Izu-Bonin-Mariana margin and insights regarding global nitrogen subduction. *Geochem. Geophys. Geosyst.* **5**, Q03115.

Salters V. J. M. and Stracke A. (2004) Composition of the depleted mantle. *Geochem. Geophys. Geosyst.* **5**.

Sano Y. and Williams S. N. (1996) Fluxes of mantle and subducted carbon along convergent plate boundaries. *Geophys. Res. Lett.* **23**, 2749–2752.

Savov I. P., Ryan J. G., D'Antonio M. and Fryer P. (2007) Shallow slab fluid release across and along the Mariana arc-basin system: Insights from geochemistry of serpentinized peridotites from the Mariana fore arc. *J. Geophys. Res. Solid Earth* **112**, 2007.

Shaw A. M., Hilton D. R., Fischer T. P., Walker J. A. and Alvarado G. E. (2003) Contrasting He–C relationships in Nicaragua and Costa Rica: insights into C cycling through subduction zones☆. *Earth Planet. Sci. Lett.* **214**, 499–513.

Shen J., Li S.-G., Wang S.-J., Teng F.-Z., Li Q.-L. and Liu Y.-S. (2018) Subducted Mg-rich carbonates into the deep mantle wedge. *Earth Planet. Sci. Lett.* **503**, 118–130.

Shepherd J. B. and Robson G. R. (1967) The source of the T phase recorded in the eastern Caribbean on October 24, 1965. *Bull. Seismol. Soc. Am.* **57**, 227–234.

Shillington D. J., Avendonk H. J. A. V., Holbrook W. S., Kelemen P. B. and Hornbach M. J. (2004) Composition and structure of the central Aleutian island arc from arc-parallel wide-angle seismic data. *Geochem. Geophys. Geosyst.* **5**.

Shirey S., Smit K., Pearson G., Walter M., Aulbach S., Brenker F., Bureau H., Burnham A., Cartigny P., Chacko T., Frost D., Hauri E., Jacob D., Jacobsen S., Kohn S., Luth R., Mikhail S., Navon O., Nestola F. and Weiss Y. (2019). *Diamonds and the Mantle Geodynamics of Carbon: Deep Mantle Carbon Evolution from the Diamond Record*. Cambridge University Press, pp. 89–128.

Sigurdsson H. and Shepherd J. (1974) Amphibole-bearing basalts from the submarine volcano Kick'em-Jenny in the Lesser Antilles island arc. *Bulletin Volcanologique* **38**, 891.

Speed R. C., Smith-Horowitz P., Perch-Nielsen K. and Sanfilippo A. (1993) *Southern Lesser Antilles Arc Platform: Pre-Late Miocene Stratigraphy, Structure, and Tectonic Evolution*. Geological Society of America.

Steiger R. H. and Jäger E. (1977) Subcommission on geochronology: Convention on the use of decay constants in geo- and cosmochronology. *Earth Planet. Sci. Lett.* **36**, 359–362.

Storey M., Duncan R. and Swisher C. (2007) Paleocene-Eocene thermal maximum and the opening of the Northeast Atlantic. *Science* **316**, 587–589.

Sun J., Zhu X.-K., Belshaw N. S., Chen W., Doroshkevich A. G., Luo W.-J., Song W.-L., Chen B.-B., Cheng Z.-G., Li Z.-H., Wang Y., Kynicky J. and Henderson G. M. (2021) Ca isotope systematics of carbonatites: insights into carbonatite source and evolution. *Geochem. Perspect. Lett.*, **17**, 11–15.

Syracuse E. M. and Abers G. A. (2006) Global compilation of variations in slab depth beneath arc volcanoes and implications. *Geochem. Geophys. Geosyst.* **7**.

Syracuse E. M., van Keken P. E. and Abers G. A. (2010) The global range of subduction zone thermal models. *Phys. Earth Planet. Inter.* **183**, 73–90.

Teng F.-Z. (2017) Magnesium isotope geochemistry. *Rev. Mineral. Geochem.* **82**, 219–287.

Teng F.-Z., Hu Y. and Chauvel C. (2016) Magnesium isotope geochemistry in arc volcanism. *PNAS* **113**, 7082–7087.

Tibaldi A. and Bonali F. (2017) Intra-arc and back-arc volcano-tectonics: Magma pathways at Holocene Alaska-Aleutian volcanoes. *Earth-Sci. Rev.* **167**, 1–26.

Tipper E. T., Schmitt A.-D. and Gussone N. (2016) *Global Ca Cycles: Coupling of Continental and Oceanic Processes. Calcium Stable Isotope Geochemistry*. Springer, pp. 173–222.

Turner S., Hawkesworth C., Van Calsteren P., Heath E., Macdonald R. and Black S. (1996) U-series isotopes and destructive plate margin magma genesis in the Lesser Antilles. *Earth Planet. Sci. Lett.* **142**, 191–207.

Vaca L., Alvarado A. and Corrales R. (1989) Calcite deposition at Miravalles geothermal field Costa Rica. *Geothermics* **18**, 305–312.

Valdes M. C., Debaille V., Berger J. and Armytage R. M. (2019) The effects of high-temperature fractional crystallization on calcium isotopic composition. *Chem. Geol.* **509**, 77–91.

Valdes M. C., Moreira M., Foriel J. and Moynier F. (2014) The nature of Earth's building blocks as revealed by calcium isotopes. *Earth Planet. Sci. Lett.* **394**, 135–145.

van Keken P. E., Hacker B. R., Syracuse E. M. and Abers G. A. (2011) Subduction factory: 4. Depth-dependent flux of H2O from subducting slabs worldwide. *J. Geophys. Res.*, 116.

Van Soest M. C., Hilton D. R. and Kreulen R. (1998) Tracing crustal and slab contributions to arc magmatism in the lesser antilles island arc using helium and carbon relationships in geothermal fluids. *Geochim. Cosmochim. Acta* **62**, 3323–3335.

Wang S.-J., Teng F.-Z. and Li S.-G. (2014) Tracing carbonate–silicate interaction during subduction using magnesium and oxygen isotopes. *Nat. Commun.* **5**, 5328.

Wang X., Wang Z., Liu Y., Park J. W., Kim J., Li M. and Zou Z. (2021) Calcium stable isotopes of Tonga and Mariana arc lavas: Implications for slab fluid-mediated carbonate transfer in cold subduction zones e2020JB020207. *J. Geophys. Res. Solid Earth*.

Wang X. J., Chen L. H., Hofmann A. W., Hanyu T., Kawabata H., Zhong Y., Xie L. W., Shi J. H., Miyazaki T., Hirahara Y.,

Takahashi, Senda R., Chang Q., Vaglarov B. S. and Kimura J. I. () Recycled ancient ghost carbonate in the Pitcairn mantle plume. *PNAS* **115**, 8682–8687.

Wang Y., He Y., Wu H., Zhu C., Huang S. and Huang J. (2019) Calcium isotope fractionation during crustal melting and magma differentiation: Granitoid and mineral-pair perspectives. *Geochim. Cosmochim. Acta* **259**, 37–52.

Wegner W., Wörner G., Harmon R. S. and Jicha B. R. (2011) Magmatic history and evolution of the Central American Land Bridge in Panama since Cretaceous times. *Bulletin* **123**, 703–724.

Wombacher F., Rehkämper M., Mezger K., Bischoff A. and Münker C. (2008) Cadmium stable isotope cosmochemistry. *Geochim. Cosmochim. Acta* **72**, 646–667.

Woodhead J., Eggins S. and Gamble J. (1993) High field strength and transition element systematics in island arc and back-arc basin basalts: evidence for multi-phase melt extraction and a depleted mantle wedge. *Earth Planet. Sci. Lett.* **114**, 491–504.

Yang W., Teng F.-Z., Zhang H.-F. and Li S.-G. (2012) Magnesium isotopic systematics of continental basalts from the North China craton: implications for tracing subducted carbonate in the mantle. *Chem. Geol.* **328**, 185–194.

Yogodzinski G. M., Brown S. T., Kelemen P. B., Vervoort J. D., Portnyagin M., Sims K. W., Hoernle K., Jicha B. R. and Werner R. (2015) The role of subducted basalt in the source of island arc magmas: evidence from seafloor lavas of the western Aleutians. *J. Petrol.* **56**, 441–492.

Yogodzinski G., Kay R., Volynets O., Koloskov A. and Kay S. (1995) Magnesian andesite in the western Aleutian Komandorsky region: implications for slab melting and processes in the mantle wedge. *Geol. Soc. Am. Bull.* **107**, 505–519.

Young E. D., Galy A. and Nagahara H. (2002) Kinetic and equilibrium mass-dependent isotope fractionation laws in nature and their geochemical and cosmochemical significance. *Geochim. Cosmochim. Acta* **66**, 1095–1104.

Zhang H., Wang Y., He Y., Teng F. Z., Jacobsen S. B., Helz R. T., Marsh B. D. and Huang S. (2018) No measurable calcium isotopic fractionation during crystallization of Kilauea Iki lava lake. *Geochem. Geophys. Geosyst.* **19**, 3128–3139.

Zhu H., Du L., Li X., Zhang Z. and Sun W. (2020a) Calcium isotopic fractionation during plate subduction: Constraints from back-arc basin basalts. *Geochim. Cosmochim. Acta* **270**, 379–393.

Zhu H., Liu F., Li X., Wang G., Zhang Z. and Sun W. (2018) Calcium isotopic compositions of normal Mid-Ocean Ridge Basalts from the Southern Juan de Fuca Ridge. *J. Geophys. Res. Solid Earth* **123**, 1303–1313.

Zhu H., Liu F., Li X., Yajun A., Nan X., Du L., Huang F., Sun W. and Zhang Z. (2020b) Significant $\delta^{44/40}$Ca variations between carbonate- and clay-rich marine sediments from the Lesser Antilles forearc and implications for mantle heterogeneity. *Geochim. Cosmochim. Acta* **276**, 239–257.

Associate editor: Shichun Huang